Article

Neuron

Synaptogyrin-3 Mediates Presynaptic Dysfunction Induced by Tau

Highlights

- Pathological Tau accumulates on synaptic vesicles in Alzheimer's disease brain
- Tau binds to synaptic vesicles via the transmembrane protein Synaptogyrin-3
- Synaptogyrin-3 mediates Tau-induced vesicle clustering at presynaptic terminals
- Synaptogyrin-3 reduction restores neurotransmitter release in fly and mouse neurons

Authors

Joseph McInnes, Keimpe Wierda, An Snellinx, ..., Joris De Wit, Lujia Zhou, Patrik Verstreken

Correspondence

patrik.verstreken@kuleuven.vib.be

In Brief

Tau mislocalizes to presynaptic terminals in human disease conditions. Here McInnes et al. show that interaction between Tau and the presynaptic vesicle protein Synaptogyrin-3 restricts synaptic vesicle mobility, driving defects in neurotransmission in fly and mouse models of Tauopathy.

McInnes et al., 2018, Neuron *97*, 823–835
February 21, 2018
https://doi.org/10.1016/j.neuron.2018.01.022

CellPress

Neuron
Article

Synaptogyrin-3 Mediates Presynaptic Dysfunction Induced by Tau

Joseph McInnes,[1,2,9] Keimpe Wierda,[1,2] An Snellinx,[1,2] Laura Bounti,[1,2] Yu-Chun Wang,[1,2] Ilie-Cosmin Stancu,[3,4] Nuno Apóstolo,[1,2] Kris Gevaert,[5,6] Ilse Dewachter,[3,4] Tara L. Spires-Jones,[7] Bart De Strooper,[1,2,8] Joris De Wit,[1,2] Lujia Zhou,[1,2] and Patrik Verstreken[1,2,10,*]

[1]VIB-KU Leuven Center for Brain & Disease Research, 3000 Leuven, Belgium
[2]Department of Neurosciences and Leuven Brain Institute, KU Leuven, 3000 Leuven, Belgium
[3]Institute of Neuroscience, Alzheimer Dementia Group, Catholic University of Louvain, 1200 Brussels, Belgium
[4]Biomedical Research Institute, Hasselt University, 3500 Hasselt, Belgium
[5]VIB-UGent Center for Medical Biotechnology, 9000 Ghent, Belgium
[6]Department of Biochemistry, Ghent University, 9000 Ghent, Belgium
[7]UK Dementia Research Institute, Euan MacDonald Centre, and Centre for Dementia Prevention, Edinburgh Neuroscience, University of Edinburgh, Edinburgh EH8 9JZ, UK
[8]Dementia Research Institute, University College London, London WC1E 6BT, UK
[9]Present address: Jan and Dan Duncan Neurological Research Institute at Texas Children's Hospital and Baylor College of Medicine, Houston, TX 77030, USA
[10]Lead Contact
*Correspondence: patrik.verstreken@kuleuven.vib.be
https://doi.org/10.1016/j.neuron.2018.01.022

SUMMARY

Synaptic dysfunction is an early pathological feature of neurodegenerative diseases associated with Tau, including Alzheimer's disease. Interfering with early synaptic dysfunction may be therapeutically beneficial to prevent cognitive decline and disease progression, but the mechanisms underlying synaptic defects associated with Tau are unclear. In disease conditions, Tau mislocalizes into pre- and postsynaptic compartments; here we show that, under pathological conditions, Tau binds to presynaptic vesicles in Alzheimer's disease patient brain. We define that the binding of Tau to synaptic vesicles is mediated by the transmembrane vesicle protein Synaptogyrin-3. In fly and mouse models of Tauopathy, reduction of Synaptogyrin-3 prevents the association of presynaptic Tau with vesicles, alleviates Tau-induced defects in vesicle mobility, and restores neurotransmitter release. This work therefore identifies Synaptogyrin-3 as the binding partner of Tau on synaptic vesicles, revealing a new presynapse-specific Tau interactor, which may contribute to early synaptic dysfunction in neurodegenerative diseases associated with Tau.

INTRODUCTION

Tau pathology is associated with more than 20 neurodegenerative diseases, including Alzheimer's disease (Wang and Mandelkow, 2016). Hyperphosphorylation or mutation of the microtubule-associated protein Tau is common to all of these diseases, collectively termed Tauopathies, and filamentous inclusions of hyperphosphorylated Tau are hallmark pathologies of Alzheimer's disease and other Tauopathies (Ballatore et al., 2007). Tau pathology is not merely a by-product of other pathological pathways, but it is a key mediator of neurotoxicity itself. In mouse models of familial Alzheimer's disease modeling excessive β-amyloid production, reduction of endogenous Tau ameliorates neurotoxicity and cognitive deficits (Roberson et al., 2007). Moreover, mutations in the Tau-encoding *MAPT* locus are causative of frontotemporal dementia with parkinsonism linked to chromosome 17 (FTDP-17) (Hutton et al., 1998), and Tau duplications or haplotypes that have elevated Tau expression levels are associated with dementia (Allen et al., 2014; Caffrey and Wade-Martins, 2007; Labbé et al., 2016; Le Guennec et al., 2017; Winder-Rhodes et al., 2015). These findings support Tau as an executor of neuronal toxicity and degeneration in human disease.

In physiological conditions, Tau is expressed in neurons and is bound to axonal microtubules. In pathological conditions, however, mutations in Tau (in FTDP-17) or abnormal phosphorylation of Tau (including in sporadic Alzheimer's disease) decrease its microtubule-binding affinity (Hong et al., 1998; Wang and Mandelkow, 2016), leading to its dissociation from axonal microtubules and subsequent mislocalization to synapses (Spires-Jones and Hyman, 2014; Tai et al., 2012, 2014). In Alzheimer's disease patients and animal models of Tauopathy, Tau mislocalization to synaptic compartments correlates well with the onset of synaptic dysfunction and cognitive decline (DeKosky and Scheff, 1990; Spires-Jones and Hyman, 2014; Yoshiyama et al., 2007). Importantly, synaptic defects are associated with soluble forms of Tau preceding Tau tangle formation in early disease stages (Koss et al., 2016), in agreement with studies showing that soluble Tau is sufficient to drive neuronal dysfunction in the absence of Tau tangles (Crimins et al., 2012; Polydoro et al., 2014; Rocher et al., 2010; Santacruz et al., 2005). These

findings highlight a key role of soluble (monomeric or oligomeric) Tau in perturbing synaptic function in early disease stages, which likely contributes to subsequent synapse loss and neurodegeneration.

While growing evidence has implicated soluble Tau dysfunction in causing neurotoxicity, less understood are the precise mechanisms by which Tau impairs neuronal function. Previous work has elucidated functions of pathological Tau in contributing to postsynaptic dysfunction on account of its mislocalization to dendritic spines and interference with glutamate receptor organization (Hoover et al., 2010; Ittner et al., 2010; Zhao et al., 2016). However, in addition to its postsynaptic localization, pathological Tau is also present in presynaptic compartments (Tai et al., 2012, 2014; Zhou et al., 2017), suggesting that Tau function at the presynapse may also contribute to disease pathogenesis. A presynaptic function of Tau is also pertinent given that neurodegeneration is thought to begin with the loss of presynaptic terminals and proceed retrogradely in a dying-back process (Yoshiyama et al., 2007). Moreover, in fly and rat neurons, Tau can interfere with neurotransmitter release by associating with synaptic vesicles at presynaptic terminals (Zhou et al., 2017). Together, these findings suggest a critical role for synapse-localized Tau in contributing to neurotoxicity in early disease stages.

In this work, we show that pathological, hyperphosphorylated Tau species accumulate on presynaptic vesicles isolated from Alzheimer's disease patient brains, suggesting this pathway contributes to synaptic dysfunction in human disease. Using unbiased proteomic and genetic approaches, we find that the transmembrane synaptic vesicle protein Synaptogyrin-3 mediates the association of Tau with synaptic vesicles *in vitro* and *in vivo*. Reduction of *Drosophila* Synaptogyrin or murine Synaptogyrin-3 levels in neurons of fly and mouse models of Tauopathy reduces the association of Tau with synaptic vesicles, and, subsequently, it rescues Tau-induced defects in vesicle mobility and neurotransmitter release. Our findings identify Synaptogyrin-3 as a novel Tau interactor that mediates Tau-induced synaptic dysfunction, providing important insights into Tau biology and opening new avenues for specifically targeting early presynaptic dysfunction in Tauopathies.

RESULTS

Synaptogyrin-3 Is a Physical and Genetic Interactor of Tau

We and others previously described the localization of pathological hyperphosphorylated Tau to presynaptic terminals of Alzheimer's disease patient brains (Tai et al., 2012, 2014; Zhou et al., 2017), and our recent work demonstrated that presynaptically localized Tau binds to fly and rodent synaptic vesicles (SVs) via its N-terminal domain (Zhou et al., 2017). To assess the possible relevance of Tau association with SVs in human disease, we biochemically fractionated post-mortem brain tissue from Alzheimer's disease patients or non-demented control subjects to isolate SVs (Figures S1A and S1B). Examining a cohort of 15 patients (Table S1), we observed enrichment of hyperphosphorylated Tau species in the SV fractions from Alzheimer's disease patient brains using antibodies recognizing disease-associated phospho-Tau epitopes (AT8 and PHF-1) or total Tau (DAKO) (Figure 1; Figure S1C). We also detected some native Tau on SVs from healthy control subjects, but this amount was on average 2- to 3-fold increased on SVs from Alzheimer's patient brain (Figure 1B; see also Discussion). Furthermore, Tau on SVs from Alzheimer's disease brain was predominantly hyperphosphorylated and oligomeric species, which are known to be highly toxic in the brain (Wang and Mandelkow, 2016). The amount of Tau on SVs was correlated with the diagnosis of Alzheimer's disease, but not age or gender (Figures S1D and S1E). These data suggest the association of pathological Tau species with SVs in Alzheimer's disease, warranting further exploration of this pathway as a potential contributor to Tau-induced synaptic dysfunction in human disease.

We first determined the binding mechanism of Tau to SVs in order to identify new targets to disrupt this interaction. SVs are comprised of the vesicle membrane, integral transmembrane SV proteins, and peripheral SV-associated proteins (Takamori et al., 2006). We first assessed whether protein-protein interactions or membrane lipid interactions mediate the association of Tau with SVs. We isolated SVs from mouse brain (Figures S2A and S2B), and we performed limited proteolysis by incubation with trypsin, which degrades all peripheral SV-associated proteins and the cytoplasmic domains of transmembrane SV proteins but leaves the membrane lipid bilayer intact (Figures 2A and 2B). We then incubated untreated or trypsinized SVs with recombinant human Tau purified from bacteria (Figures S2C and S2D). Following incubation with Tau, SVs were pelleted by ultracentrifugation, and the binding of Tau to SVs was assessed by immunoblotting for Tau in the SV pellet. The co-sedimentation assay accurately reflects direct Tau binding to SVs and is not influenced by Tau aggregation (Zhou et al., 2017). In the co-sedimentation assay, Tau bound to untreated SVs, but this binding was largely lost upon proteolysis of SV proteins (Figures 2C and 2D), indicating that SV proteins are required for Tau binding to SVs. Following sedimentation, the amount of Tau in the supernatants was similar, showing that there is no residual trypsin activity following proteolysis of SVs (Figure S2E). In agreement, we also did not detect Tau binding to synthetic protein-free liposomes, which were similar in size and lipid composition to SVs (Figure S2F). Thus, protein-protein interactions underlie the binding of Tau to SVs.

To further delineate whether Tau binds to SVs via interaction with transmembrane SV proteins or peripheral SV-associated proteins, we performed carbonate stripping of SVs. This manipulation removes peripheral SV-associated proteins but leaves transmembrane SV proteins intact (Figure 2E). When introduced into the co-sedimentation assay, Tau bound equally well to untreated and carbonate-stripped SVs (Figures 2F and 2G), indicating that peripheral SV-associated proteins are dispensable for binding. Together, these data indicate that Tau binds to SVs via interaction with transmembrane SV proteins.

We then utilized an unbiased proteomics approach to identify the transmembrane SV proteins that bind Tau (Figure 3A). We performed high-detergent lysis of isolated SVs to solubilize SV proteins, and we performed a co-immunoprecipitation (coIP) reaction using purified recombinant Tau^{FL}-His or $Tau^{\Delta N}$-His as bait (Figures S2C and S2D), followed by mass spectrometry analysis to identify bound proteins. The N-terminal domain of Tau is

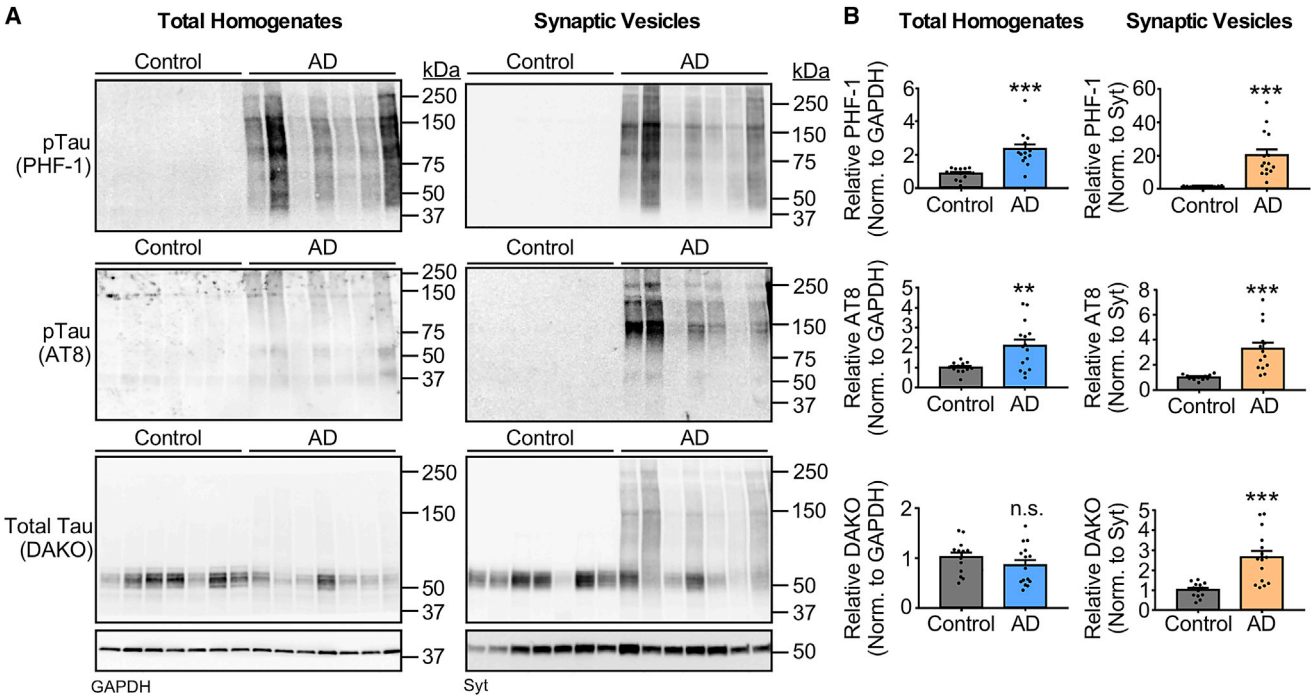

Figure 1. Pathological Tau Species Accumulate on SVs Isolated from Alzheimer's Disease Patient Brains

SVs were isolated from post-mortem brain tissue of control subjects or Alzheimer's disease (AD) patients, and they were assessed for total Tau levels (DAKO antibody) and phospho-Tau (pTau) levels using the AT8 antibody (phospho-Ser^{202}/Thr^{205} epitope) or PHF-1 antibody (phospho-Ser^{396}/Ser^{404} epitope) by immunoblotting.

(A) Representative immunoblots directly comparing the amount of pTau and total Tau in total homogenates and SV fractions from AD patients or controls, showing the presence of both monomeric (migrating around 50 kDa) as well as oligomeric (migrating $\geq$100 kDa) Tau/pTau species accumulating on SVs in AD patient brain. The cytosolic marker GAPDH and SV marker Synaptotagmin-1 (Syt) are used as loading controls for total homogenates and SV fractions, respectively.

(B) Quantifications of immunoblots comparing pTau or total Tau levels in control and AD patient brain in either total homogenate or SV fractions, normalized to loading controls.

Graphs depict mean ± SEM (n = 13 non-demented control subjects, n = 15 AD patients; Student's t test, $^{**}p < 0.01$ and $^{***}p < 0.001$; n.s., not significant). See also Figure S1 and Table S1.

required for binding to SVs (Zhou et al., 2017), and thus the interactor of Tau on SVs should bind full-length Tau (Tau^{FL}), but not N-terminally truncated Tau ($Tau^{\Delta N}$). Using this approach, we identified 8 SV proteins as potential interactors of Tau (Figure 3B; Table S2), but only one protein is both transmembrane and specific to the N terminus of Tau: Synaptogyrin-3 (Syngr3).

Syngr3 is an SV-specific protein of unknown function that has four transmembrane domains with cytoplasmic exposed N- and C-terminal tails (Kedra et al., 1998). Syngr3 is the only candidate that fits our criteria as a potential interactor of Tau *in vitro*; nevertheless, we tested whether *Drosophila* homologs of any of the 8 SV proteins identified in our proteomics approach show a genetic interaction with Tau *in vivo*. For this, we crossed flies expressing FTDP-17 clinical mutant Tau^{P301L} to loss-of-function alleles or small hairpin RNA (shRNA) constructs for the *Drosophila* homologs of these 8 candidate interactors, and we measured colocalization of Tau with SVs as a readout of Tau-SV association *in vivo* (Figures 3C and 3D). In third-instar *Drosophila* larvae expressing human Tau carrying FTDP-17 clinical mutations (P301L, V337M, or R406W) in motor neurons, mutant Tau dissociated from axonal microtubules and relocalized to presynaptic boutons at neuromuscular junctions (NMJs). At boutons, Tau colocalized with SVs that organized in a ring-like pattern in the periphery of the bouton (Figures 4A and 4B), which was quantified using the Pearson co-localization coefficient between Tau and SVs immunolabeled with anti-Cysteine String Protein (CSP) antibodies. We found that Tau^{P301L} showed a diffuse pattern when we lowered the expression level of Synaptogyrin (Syngr, the single *Drosophila* homolog of Syngr3; Stevens et al., 2012), but not any other candidate interactor (Figures 3D, 4A, and 4B). Similarly, two other pathogenic FTDP-17 Tau mutants also showed diffuse localization at boutons when Syngr expression was lowered (Figure 4C). Both heterozygous loss (50% reduction) and shRNA-mediated knockdown (90% reduction; Figures S3A and S3B) of Syngr were effective to cause dissociation of Tau from SVs to a similar extent as genetically deleting the N-terminal SV binding domain of Tau (expression of $Tau^{\Delta N}$) (Figures 3D and 4A–4C), indicating that partial loss of Syngr is sufficient to reduce Tau-SV binding *in vivo* at *Drosophila* NMJs.

To test if Syngr is required for the direct physical interaction of Tau with SVs, we isolated SVs from wild-type (WT) or *syngr*

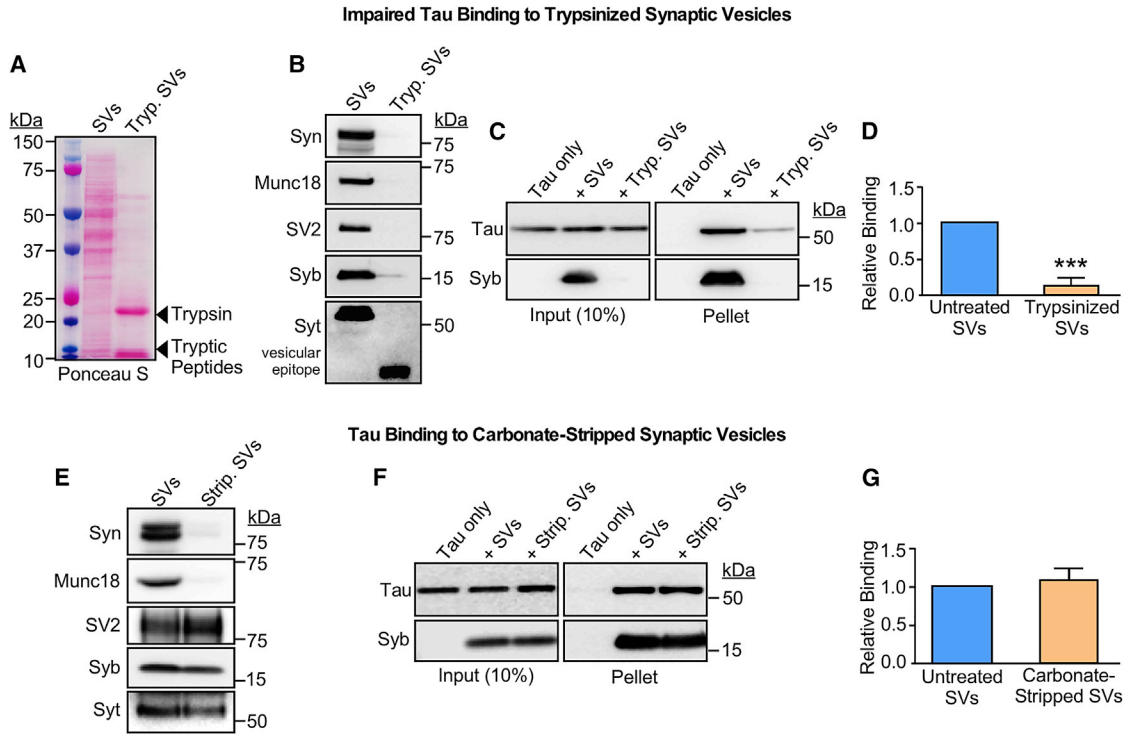

Figure 2. Tau Binds to SVs via Interaction with Transmembrane SV Proteins

(A–D) Tau binding to SVs requires SV proteins.

(A) Ponceau S staining of fractions taken during trypsin digestion of SVs shows proteolysis of SV proteins by trypsin.

(B) Immunoblotting of trypsinized SVs shows proteolytic degradation of the SV-associated proteins Synapsin (Syn) and Munc18 and degradation of the cytoplasmic domains of the transmembrane SV proteins SV2, Synaptobrevin-2 (Syb) (cytoplasmic epitopes), and Synaptotagmin-1 (Syt) (intravesicular epitope).

(C) Representative immunoblots from co-sedimentation assay with purified recombinant human Tau-His and untreated or trypsinized SVs. Immunoblotting for Tau (anti-His antibody) in the SV pellet assesses binding to SVs, as quantified in (D). Graph depicts mean ± SD (n = 3 experiments; Student's t test, ***$p < 0.001$).

(E–G) Peripheral SV-associated proteins are dispensable for Tau binding to SVs.

(E) Immunoblotting of untreated or carbonate-stripped SVs confirms removal of the SV-associated proteins Syn and Munc18 but retention of the transmembrane SV proteins SV2, Syb, and Syt (cytoplasmic epitopes).

(F) Representative immunoblots from co-sedimentation assay assessing Tau binding to untreated or carbonate-stripped SVs, as quantified in (G).

Graph depicts mean ± SD from two independent experiments. See also Figure S2.

knockout (KO) adult fly brains (Figures S3C and S3D). In the co-sedimentation assay, recombinant human Tau bound to wild-type SVs, but binding to *syngr* KO SVs was severely reduced (Figures 4D and 4E). These results complement our findings at NMJs *in vivo*, where the reduction of Syngr caused the diffuse localization of pathogenic Tau (Figures 4A–4C). Taken together, these data indicate that the physical interaction between Tau and Syngr is the principle mechanism underlying the binding of Tau to SVs.

Reduction of Syngr Rescues Tau-Induced Presynaptic Dysfunction in *Drosophila*

When Tau binds to SVs, they become crosslinked and less mobile, causing defects in the recruitment of a sufficient number of vesicles to maintain neurotransmitter release during sustained activity (Zhou et al., 2017). We show here that Syngr mediates the association of Tau with SVs, and we therefore assessed whether the reduction of Syngr is sufficient to rescue Tau-induced presynaptic defects. As a readout of SV crosslinking, we examined the mobility of SVs at larval NMJs using a fluorescence recovery after photobleaching (FRAP) assay. In larvae expressing the live SV marker Synaptotagmin-GFP (Syt-GFP), photobleaching of a small area of SVs within a presynaptic bouton depletes Syt-GFP fluorescence from those SVs, and the recovery of fluorescence signal over time in that area therefore reflects the mobility of other SVs that diffuse in (Seabrooke et al., 2010). In comparison to controls, SV mobility at presynaptic boutons in larvae expressing three independent pathogenic Tau mutants was reduced, indicative of Tau-induced SV crosslinking (Figures 5A–5D, solid lines). In contrast, heterozygous loss of Syngr was sufficient to restore SV mobility back to control levels on all three mutant Tau backgrounds (Figures 5A–5D, dotted lines). This rescue of SV mobility was specific to pathogenic Tau-induced deficits, as $syngr^{+/-}$ alone on a WT background did not affect SV mobility (Figure 5E). Thus, Syngr-dependent binding of Tau to SVs directly impairs SV mobility at presynaptic terminals.

We next assessed whether Syngr mediates Tau-induced defects in neurotransmitter release by acquiring electrophysiological recordings at larval NMJs. Larvae expressing mutant

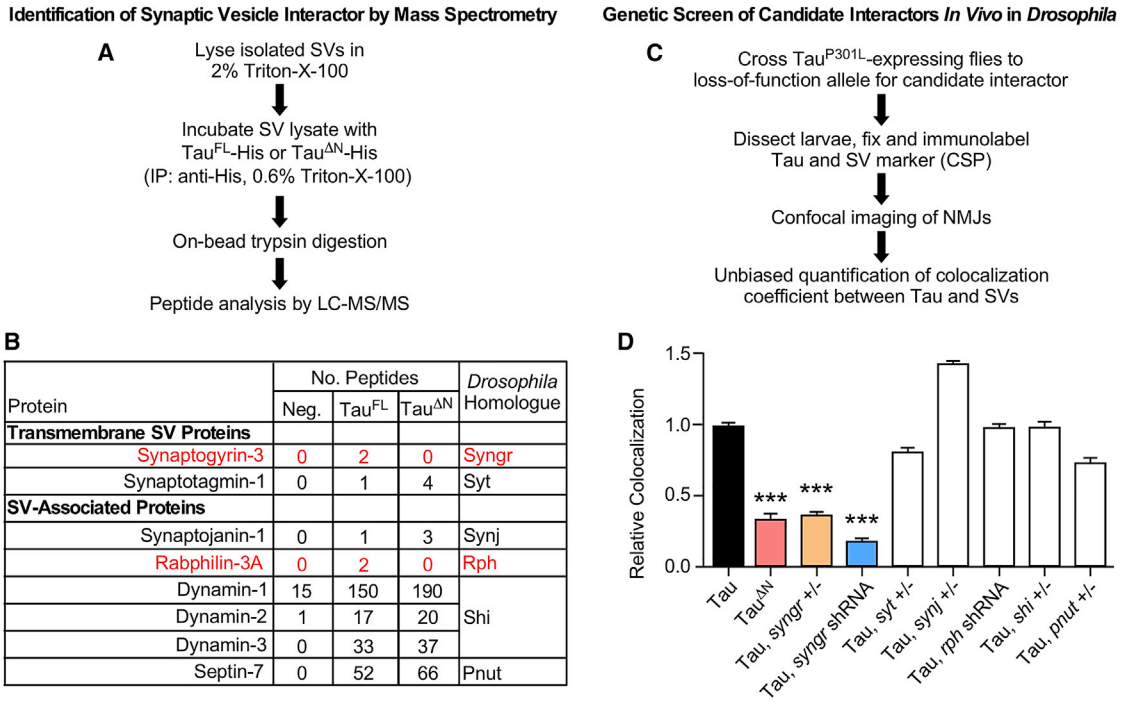

B

Protein	No. Peptides			*Drosophila* Homologue
	Neg.	Tau^{FL}	Tau$^{\Delta N}$	
Transmembrane SV Proteins				
Synaptogyrin-3	0	2	0	Syngr
Synaptotagmin-1	0	1	4	Syt
SV-Associated Proteins				
Synaptojanin-1	0	1	3	Synj
Rabphilin-3A	0	2	0	Rph
Dynamin-1	15	150	190	Shi
Dynamin-2	1	17	20	
Dynamin-3	0	33	37	
Septin-7	0	52	66	Pnut

Figure 3. Integrated Proteomic and Genetic Screens Identify Syngr3 as a Physical and Genetic Interactor of Tau

(A and B) Identification of the SV interactor of Tau by mass spectrometry.

(A) Experimental workflow of coIP of SV protein lysate with purified recombinant human Tau.

(B) Filtered results from liquid chromatography-tandem mass spectrometry (LC-MS/MS) analysis showing peptide counts from three replicates. Proteins specific to the N terminus of Tau are in red. See also Table S2 for raw dataset.

(C and D) *In vivo* follow-up genetic screen of candidate interactors in *Drosophila*.

(C) Experimental workflow to assess Tau binding to SVs (as measured by colocalization of Tau with SVs) at NMJs upon partial loss of the candidate interactors identified in (B).

(D) Quantification of relative colocalization of immunolabeled Tau and the SV marker CSP at NMJs (see Figure 4). *Drosophila* larvae express UAS-Tau^{P301L} or UAS-Tau^{P301L} ΔN under the motor neuron-specific D42-Gal4 driver.

Graph depicts mean ± SEM (n ≥ 8 NMJs per genotype from ≥4 animals per genotype; one-way ANOVA, ***p < 0.001).

Tau^{P301L} did not show apparent defects in spontaneous release or evoked release in response to short stimuli (Figure S4), but they did show impaired release during sustained activity, exhibiting progressively lower excitatory junction potential (EJP) amplitudes in response to 10-Hz stimulation for 10 min (Figures 5F–5H, blue). Upon the reduction of Syngr levels (*syngr*$^{+/-}$), however, activity-dependent release was rescued back to control levels (Figures 5F–5H, orange). Again, this rescue was specific to pathogenic Tau-induced deficits, as *syngr*$^{+/-}$ mutant larvae alone did not exhibit differences in spontaneous or evoked neurotransmitter release during short or sustained stimulation (Figures 5F–5H, gray; Figure S4). Taken together, these data support our model that presynaptically localized pathogenic Tau directly binds and crosslinks SVs via Syngr, preventing vesicle recruitment into release and ultimately attenuating neurotransmission during sustained activity.

Syngr3 Mediates Presynaptic Dysfunction in Hippocampal Neurons from a Tauopathy Mouse Model

The mammalian genome encodes four Synaptogyrins that are distantly related to Synaptophysin and Synaptoporin, all of which share a common topology of four transmembrane domains with cytoplasmic exposed N- and C-terminal tails (Kedra et al., 1998). Only Syngr1 and Syngr3 are neuron specific and present on SVs (Belizaire et al., 2004). Our proteomics screen only identified Syngr3 as a Tau interactor, and we therefore set out to test if the reduction of Syngr3 is sufficient to ameliorate synaptic dysfunction in neurons of a well-established transgenic mouse model of Tauopathy. Tau PS19 mice express human FTDP-17 clinical mutant Tau^{P301S} and show disease-relevant features of synaptic dysfunction, synapse loss, and neurodegeneration during aging (Yoshiyama et al., 2007). We first assessed if FTDP-17 mutant Tau^{P301S} localizes to presynaptic terminals in mouse hippocampal neurons. We established primary neuronal cultures from the hippocampi of embryonic day (E)17.5 non-transgenic (Non Tg) or Tau PS19 transgenic mouse embryos, allowed them to mature for 17 days "*in vitro* (DIV)", and then assessed Tau^{P301S} localization by immunofluorescence together with the presynaptic markers VGlut1 or Synapsin and the dendritic marker MAP2. Along distal axons, we observed a punctate staining of Tau^{P301S} that colocalized with VGlut1 (Figures S5A and S5B), indicative of presynaptic localization; as a control, staining of endogenous mouse Tau (mTau) in Non Tg neurons revealed a more diffusive staining pattern (Figures S5C and S5D),

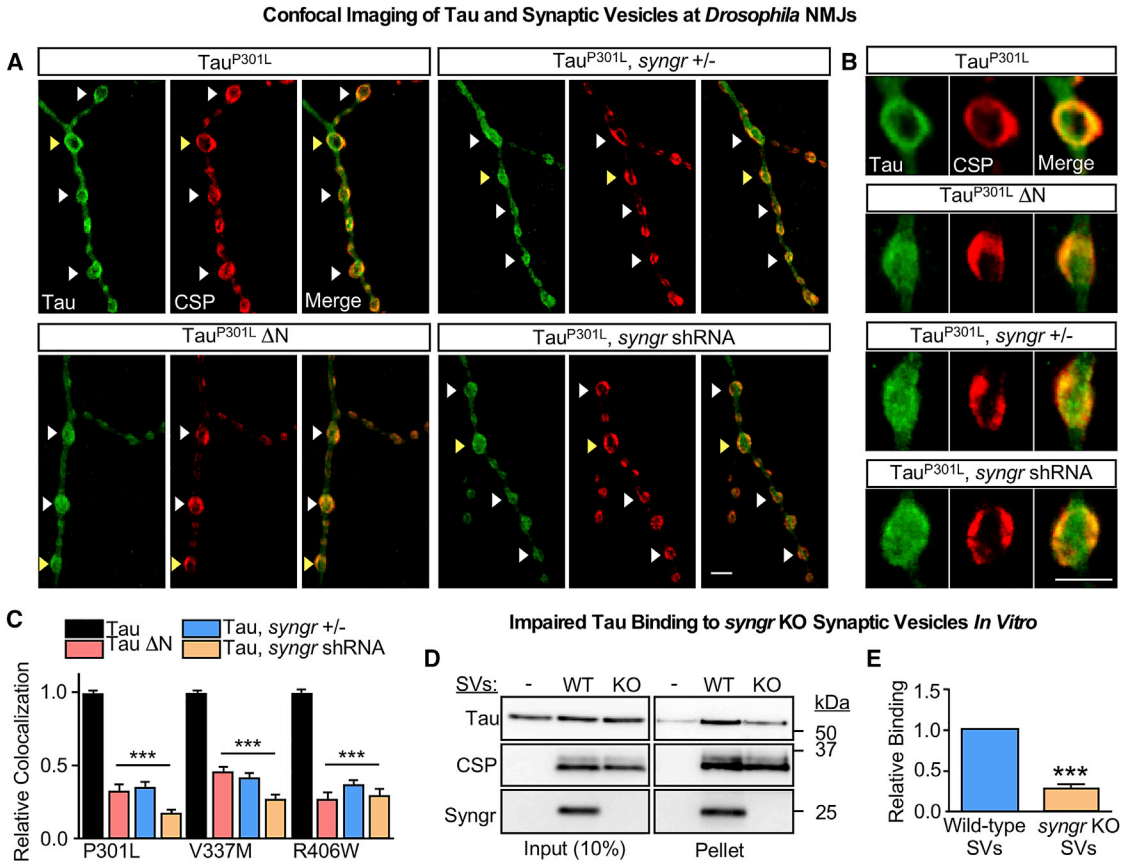

Figure 4. *Drosophila* Syngr Mediates Tau Association with SVs *In Vivo* and *In Vitro*

Drosophila larvae express pathological mutant UAS-Tau, UAS-Tau ΔN, and/or UAS-*syngr* shRNA under the control of the D42-Gal4 motor neuron promoter on a wild-type (WT) or $syngr^{+/-}$ background.

(A and B) Representative confocal images of immunolabeled Tau (DAKO antibody) and SVs (CSP antibody) at *Drosophila* NMJs (A). White arrowheads indicate presynaptic boutons. Boutons marked with yellow arrowheads are shown enlarged in (B). Scale bars, 5 μm.

(C) Plot of relative colocalization of Tau and CSP upon heterozygous loss or knockdown of Syngr in larvae expressing pathological Tau mutants. Graph depicts mean ± SEM (n = 10–28 NMJs from n ≥ 6 animals per genotype; one-way ANOVA, each condition compared to Tau only for each respective mutant genotype, ***$p < 0.001$).

(D and E) Representative immunoblots detecting recombinant human Tau-His binding to SVs (anti-His antibody) isolated from wild-type or *syngr* KO fly brains in the SV co-sedimentation assay (D), as quantified in (E). CSP serves as the loading control for SVs.

Graph depicts mean ± SD (n = 4 experiments; Student's t test, ***$p < 0.001$). See also Figure S3.

consistent with predominantly axonal localization. Thus, pathogenic mutant Tau^{P301S} localizes to presynaptic terminals in hippocampal neurons from Tau PS19 mice, recapturing this key pathogenic event also observed in human sporadic disease conditions, including Alzheimer's disease (Tai et al., 2014, 2012; Zhou et al., 2017).

We then assessed whether lowering the expression level of Syngr3 alters this punctate presynaptic localization of Tau. We produced lentiviruses expressing red fluorescent protein (RFP) as well as short hairpin sequences targeting *syngr3*, and we validated two independent shRNA constructs that result in more than a 95% reduction of Syngr3 levels but did not obviously affect neuronal viability, morphology, or synapse formation (Figures S5E–S5H). While Tau^{P301S} maintained its punctate localization to presynaptic SV clusters along the axon in scramble-transduced neurons, knockdown of Syngr3 resulted in a more diffuse staining pattern of Tau^{P301S} along the axon, with Tau^{P301S} no longer tightly associating with SV clusters (Figure 6A). As a measure of Tau association with presynaptic SV clusters, we quantified Tau^{P301S} colocalization with an SV marker along axons, which revealed a significant reduction in Tau^{P301S} association to presynaptic SV clusters upon Syngr3 knockdown (Figure 6B), whereas overall Tau levels were unaffected (Figure 6C). This reduction in Tau^{P301S} localization to presynaptic SV clusters upon the reduction of Syngr3 was specific to Tau PS19 neurons in which Tau^{P301S} had mislocalized to synapses, as the reduction of Syngr3 in Non Tg neurons did not affect endogenous mTau localization, consistent with a predominantly axonal localization of native Tau that largely precludes its association with Syngr3 in normal conditions (Figures S5I and S5J). Together, these data indicate Syngr3-dependent association of presynaptic Tau with SVs in pathogenic conditions.

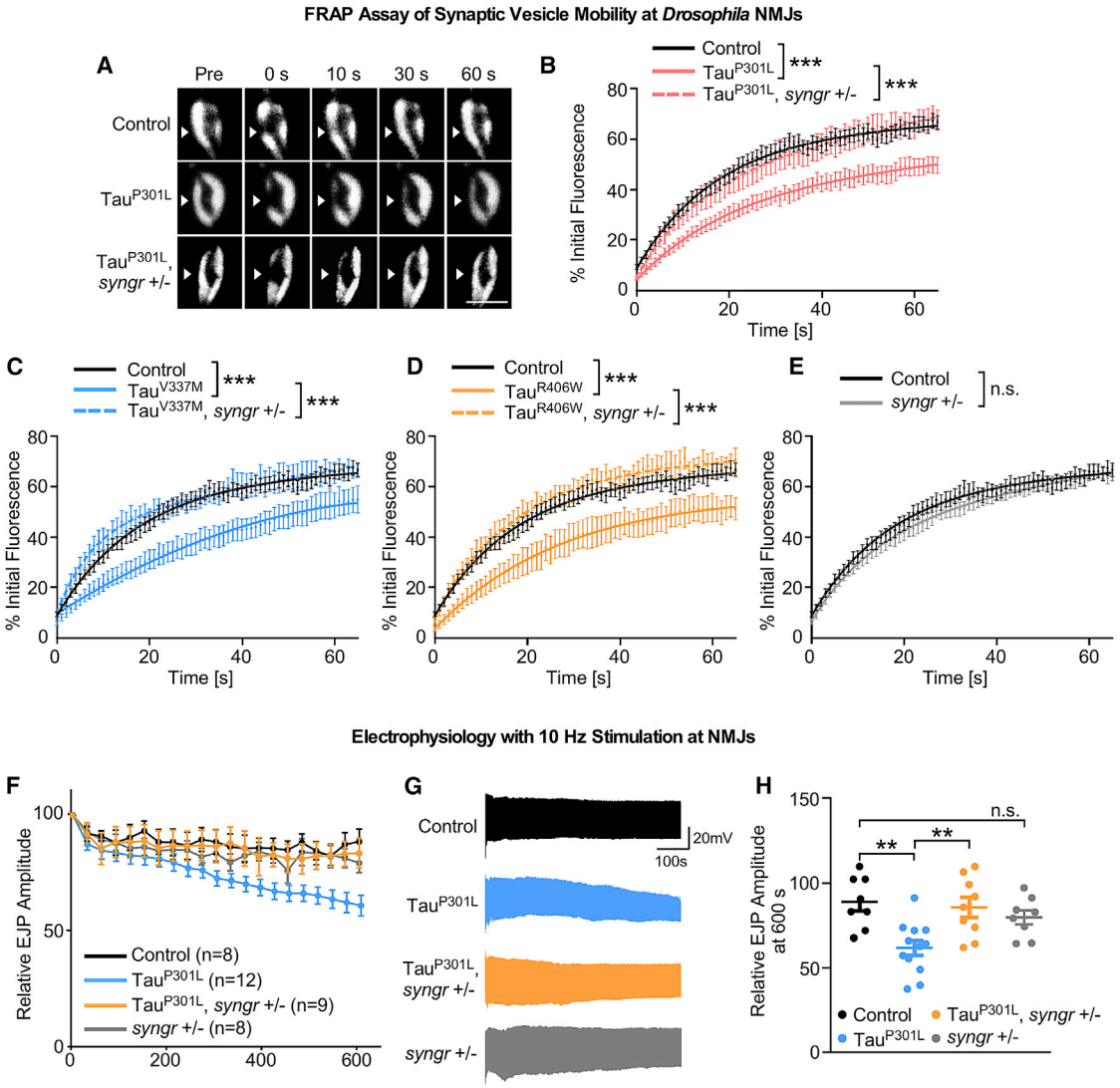

Figure 5. Reduction of Syngr Rescues Tau-Induced Defects in SV Mobility and Neurotransmitter Release at *Drosophila* Neuromuscular Junctions

(A–E) FRAP assay of SV mobility within presynaptic boutons. *Drosophila* larvae express UAS-Syt-GFP and UAS-Tau under the control of the D42-Gal4 motor neuron driver on a wild-type or $syngr^{+/-}$ background.

(A) Representative images of Syt-GFP signal before and after photobleaching show fluorescence recovery after photobleaching of small area (arrowhead) of Syt-GFP fluorescence in presynaptic bouton during 60 s. Control is D42 > Syt-GFP only. Scale bar, 5 μm.

(B–E) Plots of Syt-GFP fluorescence recovery over time fit to a double-exponential curve depicting relative vesicle mobility upon reduction of Syngr on Tau^{P301L} (B), Tau^{V337M} (C), Tau^{R406W} or wild-type backgrounds. Plots depict mean ± SEM (n = 10–15 boutons from ≥5 animals; two-way ANOVA, ***p < 0.001; n.s., not significant).

(F–H) Electrophysiological recordings of neurotransmitter release at NMJs.

(F) Plot of evoked junction potential (EJP) amplitudes in response to 10-Hz stimulation with 2 mM Ca^{2+} for 10 min in control (D42 driver only), D42 > Tau^{P301L}, Tau^{P301L} $syngr^{+/-}$, and $syngr^{+/-}$ larvae. Amplitudes are binned at 30-s intervals and normalized to the average of the first 15 s. Graph depicts mean ± SEM (n NMJ recordings indicated, 1 NMJ per animal).

(G) Representative raw data traces.

(H) Relative EJP amplitude at 600 s plotted as individual data points.

Graph depicts mean ± SEM (one-way ANOVA, **p < 0.01; n.s., not significant). See also Figure S4.

We next determined whether Syngr3-dependent association of Tau with SVs leads to reduced SV mobility in hippocampal neurons using an SV dispersion assay. At mammalian central synapses, SVs sit in tight clusters along the axon, which become more mobile and diffuse during neuronal activity (Sankaranarayanan and Ryan, 2000). Measuring the change in fluorescence intensity of a live SV marker to assess vesicle diffusion during neuronal stimulation can, therefore, serve as a measure of SV

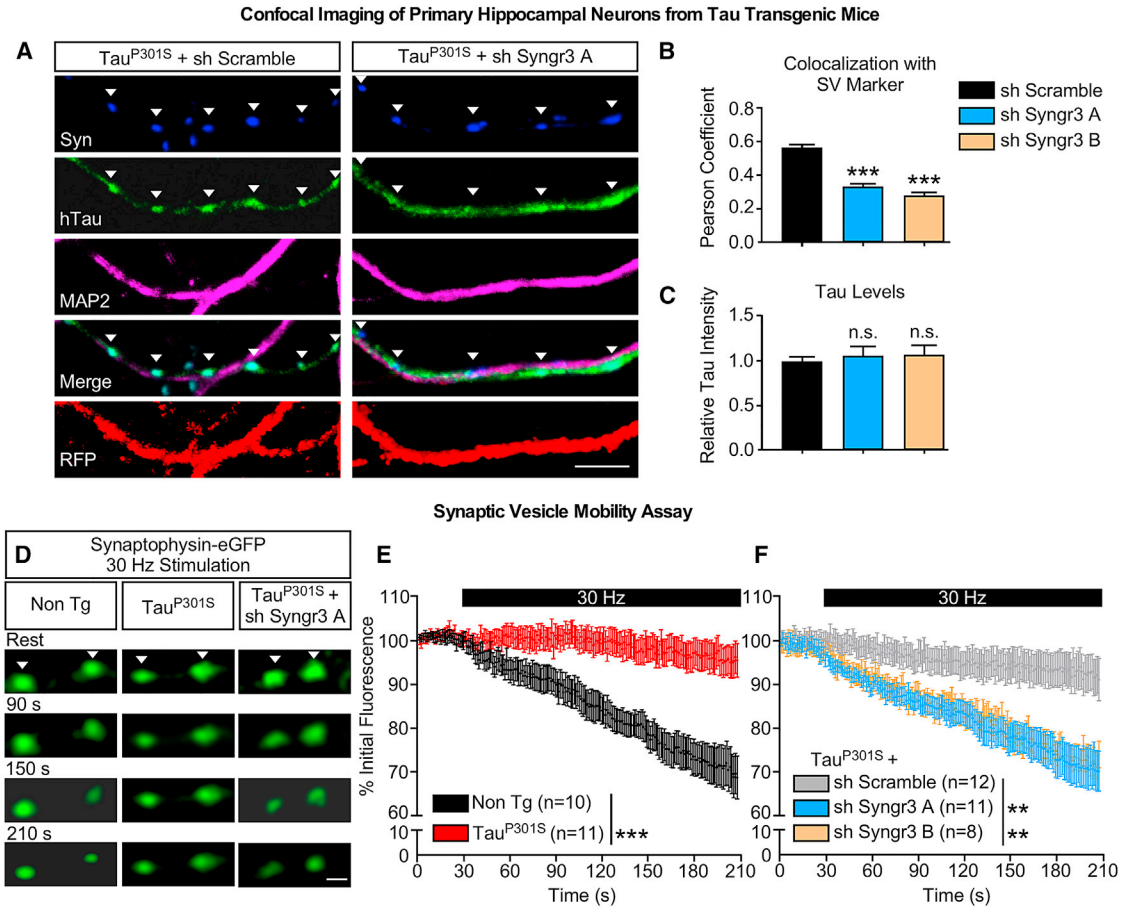

Figure 6. Syngr3 Mediates Tau Localization to Presynaptic Vesicle Clusters and Defects in SV Mobility in Primary Hippocampal Neurons from Tau Transgenic Mice

(A–C) Confocal imaging of Tau localization to presynaptic SV clusters in hippocampal neurons.

(A) Representative confocal images of Tau^{P301S} neurons (at DIV17) transduced with lentivirus co-expressing RFP and Syngr3 knockdown or scrambled control shRNAs and immunolabeled for Tau^{P301S} (hTau HT7 antibody), the SV marker Synapsin (Syn), and the dendritic marker MAP2. White arrowheads indicate presynaptic Syn puncta along axons. Scale bar, 5 μm.

(B) Quantification of Tau^{P301S} localization to SV clusters (Pearson coefficient of Tau and Syn along axons).

(C) Quantification of overall Tau^{P301S} levels (hTau intensity along axons). Graphs depict mean ± SEM (n = 85 axons from ≥24 coverslips per condition from 6 independent cultures; one-way ANOVA, ***$p < 0.001$; n.s., not significant).

(D–F) Synaptophysin-EGFP (Syph-EGFP) dispersion assay to measure SV mobility. Neurons from non-transgenic (Non Tg) littermates or Tau^{P301S} mice were transduced with lentivirus expressing Syph-EGFP only or in combination with scrambled or Syngr3 shRNA lentivirus and recorded on DIV17.

(D) Representative images of Syph-EGFP fluorescence intensity during sustained 30-Hz stimulation. White arrowheads indicate presynaptic Syph-EGFP puncta (SV clusters). Scale bar, 1 μm.

(E and F) Plots depicting change in Syph-EGFP fluorescence intensity in Non Tg and Tau^{P301S} neurons (E) or in Tau^{P301S} neurons co-transduced with shRNA virus (F). Neurons were imaged at rest for 30 s then stimulated at 30 Hz in a field stimulation chamber for 3 min during live imaging in 1-s intervals. The change in fluorescence was calculated for ≥20 puncta from ≥3 axons per coverslip then averaged to give n = 1 trace per coverslip.

Plots depict mean ± SEM (n traces/coverslips indicated from ≥5 independent cultures; two-way ANOVA, **$p < 0.01$ and ***$p < 0.001$). See also Figure S5.

mobility (Wang et al., 2014). We transduced hippocampal neurons with lentivirus expressing the SV marker Synaptophysin-EGFP (Syph-EGFP), and we performed live imaging to record changes in Syph-EGFP fluorescence intensity, which decreased in response to 30-Hz stimulation, reflecting activity-dependent SV mobilization (Figure 6D). In comparison to neurons from Non Tg littermates, neurons from Tau^{P301S} transgenic mice showed less dispersion of Syph-EGFP fluorescence during 30-Hz stimulation (Figures 6D and 6E), indicative of impaired SV mobility. However, reducing Syngr3 levels in Tau^{P301S} neurons by transduction with Syngr3 knockdown virus restored SV mobility back to control levels (Figures 6D and 6F). Knockdown of Syngr3 in Non Tg neurons did not affect SV mobility (Figure S5K); therefore, the contribution of the Tau-Syngr3 interaction to SV mobility was mostly detected in pathogenic conditions in which Tau had mislocalized to synapses and come in contact with Syngr3, having a dominant toxic effect on SV mobility. Thus, Syngr3-dependent binding of presynapse-localized Tau to SVs underlies Tau-induced defects in presynaptic vesicle mobility in pathogenic conditions.

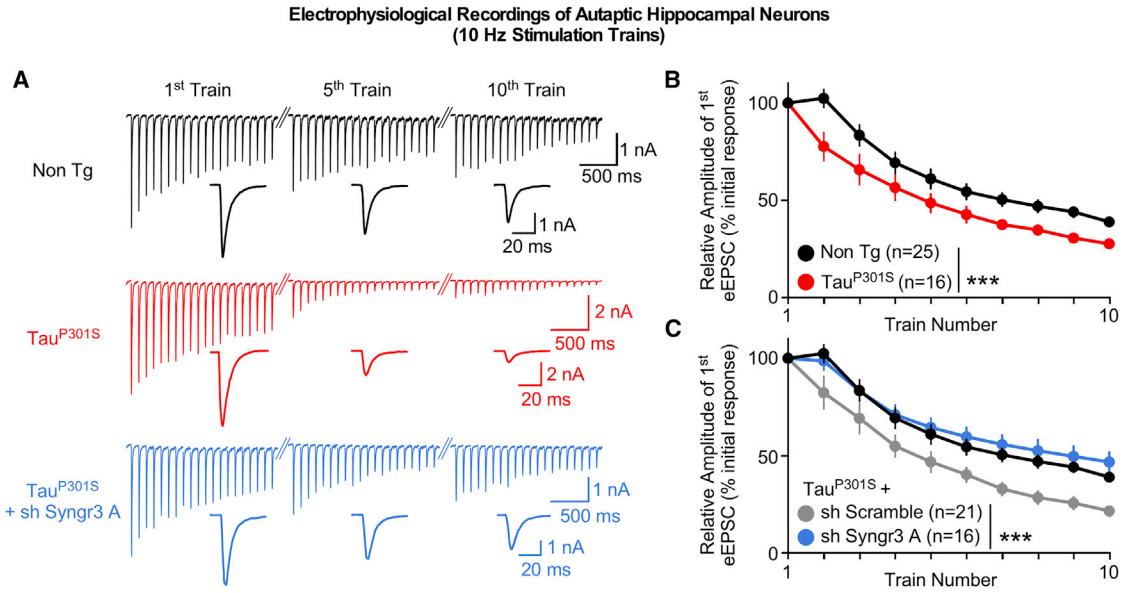

Figure 7. Reduction of Syngr3 Rescues Tau-Induced Defects in Neurotransmitter Release in Primary Hippocampal Neurons from Tau Transgenic Mice

Autaptic neuronal cultures were established from Tau^{P301S} mice or Non Tg littermates, transduced as indicated, and matured until DIV17–DIV20. Evoked release was measured by patch-clamp electrophysiology.

(A) Representative traces from electrophysiological recordings of autaptic hippocampal neurons in response to 10 consecutive high-frequency stimulation trains (10 Hz for 10 s with 30-s rest intervals, 4 mM Ca^{2+}).

(B and C) Relative first evoked excitatory postsynaptic currents (eEPSCs) for each train plotted to train number from recordings of neurons from Tau^{P301S} mice or Non Tg littermates (B) or neurons from Tau^{P301S} mice transduced with scrambled or Syngr3 knockdown lentivirus (C). Plots depict mean ± SEM (n recordings indicated from ≥3 independent cultures; some error bars too small to be seen; two-way ANOVA, ***$p < 0.001$). See also Figure S6.

Finally, we analyzed whether Tau-induced, Syngr3-mediated defects in SV mobility are functionally related to defects in neurotransmission by performing whole-cell voltage-clamp electrophysiology on DIV17–DIV20 autaptic cultures of hippocampal neurons. Tau^{P301S}-expressing neurons showed spontaneous release characteristics very similar to those we measured in Non Tg neurons (Figures S6A–S6C). However, Tau^{P301S} neurons could not sustain evoked release efficacy as well as controls during high-frequency 10-Hz stimulation trains, exhibiting progressively lower evoked excitatory postsynaptic current (eEPSC) amplitudes with each stimulation train (Figures 7A and 7B). Remarkably, reducing Syngr3 levels in Tau^{P301S} neurons by transduction with Syngr3 knockdown lentivirus was sufficient to rescue this evoked neurotransmitter release defect back to control levels (Figures 7A and 7C). This rescue was not due to altered baseline release, as spontaneous release and raw evoked amplitudes among control and rescue genotypes were similar (Figures S6A–S6D). Furthermore, knockdown of Syngr3 in Non Tg neurons did not affect evoked release during 10-Hz stimulation (Figure S6E), again indicating that Syngr3 knockdown specifically rescues Tau-induced deficits in neurotransmitter release under pathogenic conditions in which excessive amounts of Tau have trafficked to the presynaptic terminal. These data support our model that Tau crosslinking SVs via Syngr3 renders a portion of the SV pool unable to be recruited into release, ultimately lowering neurotransmitter release during sustained stimulation.

Taken together, our study identifies Syngr3 as a novel interactor of Tau, which mediates synaptic release deficits in fly and mouse models of Tauopathy by acting as the binding partner of Tau on SVs. In disease conditions, mutations or hyperphosphorylation of Tau lowers its affinity to bind axonal microtubules, causing mislocalization of Tau into presynaptic terminals where it comes in contact with the SV protein Syngr3, leading to impaired SV mobility and attenuating neurotransmitter release. By targeting Syngr3, an exclusively presynaptic SV protein, we genetically uncouple the presynaptic function of Tau from other potential pathological functions, and we reveal that specific inhibition of Syngr3-dependent Tau-SV binding ameliorates defects in synaptic function and neurotransmitter release.

DISCUSSION

Synaptic dysfunction is thought to be an early and important pathogenic step in Alzheimer's disease and other neurodegenerative diseases associated with Tau. While accumulating evidence positions Tau itself as a major executor of synaptic dysfunction, the precise mechanisms underlying Tau-induced synaptic pathology have remained elusive. Tau can act postsynaptically, where it affects glutamate receptor trafficking and organization (Hoover et al., 2010; Ittner et al., 2010), as well as presynaptically, where it clusters SVs via F-actin networks (Zhou et al., 2017). Here we define that Tau binding to the transmembrane SV protein Syngr3 mediates Tau-induced defects in SV

mobility, preventing SV recruitment into release and lowering neurotransmission. Given that Syngr3 is exclusively present on SVs, our findings present Syngr3 as a novel Tau interactor involved in Tau pathogenesis at the presynapse. This work opens new avenues for specifically targeting the presynaptic function of Tau both to selectively evaluate the contribution of this pathway to disease progression in animal models, as well as for future therapeutic approaches targeting synaptic dysfunction in Alzheimer's disease and related Tauopathies.

We validated the mechanism of Tau-SV binding as disease relevant by finding that pathological Tau species associate with SVs isolated from Alzheimer's disease patient brains, and we used *in vitro* assays of recombinant human Tau binding to isolated SVs to mechanistically define that Tau binds to SVs via its interaction with transmembrane SV proteins. Using an unbiased proteomics approach, we identified eight candidate SV interactors, but only Syngr3 was both transmembrane and specific to the N-terminal SV-binding domain of Tau and, therefore, the most likely candidate. Indeed, when we tested the genetic interaction of all eight candidates with Tau in flies, only the Syngr3 homolog reduced Tau association with SVs *in vivo*. In addition, another recent study also identified Syngr3 as a Tau interactor in an unbiased proteomics screen (Liu et al., 2016), independently confirming our result. The identification of other candidate interactors in our screen may be due to secondary interactions with other domains of Tau and could have small contributions to SV binding; nonetheless, our study identifies the interaction between the N terminus of Tau and Syngr3 to be the predominant mechanism by which Tau associates with SVs. In agreement, loss of only Syngr3 from SVs is sufficient to rescue the associated presynaptic deficits in neurons.

The mammalian genome encodes four Synaptogyrins, but only Syngr1 and Syngr3 are neuron specific and present on SVs (Belizaire et al., 2004; Kedra et al., 1998). While a redundant role of Syngr1 and Synaptophysin in synaptic plasticity has been described (Janz et al., 1999), the physiological function of Syngr3 remains to be explored. Although its function is unknown, our initial experiments suggest targeting Syngr3 therapeutically may be safe and feasible: >95% knockdown of Syngr3 in mouse neurons did not obviously affect neuron or synapse development, and it rescued Tau-induced presynaptic defects without inducing additional toxicity in the parameters we measured. Furthermore, *Drosophila syngr*-null KO flies are viable, healthy, and do not show overt defects in presynaptic function (Stevens et al., 2012). Interestingly, in our fly model, a 50% reduction (heterozygous loss) was already sufficient to rescue functional defects, suggesting only a mild reduction of Syngr3 may be effective to bring levels of Tau-SV binding below a pathogenic threshold. On one hand, this could be because many non-essential SV proteins are present in low copy number, i.e., 1–3 per SV (Takamori et al., 2006), and lowering Syngr levels by 50% may, therefore, result in a substantial a pool of SVs devoid of Syngr3. On the other hand, in our current experimental systems, the functional effects are rather mild, consistent with other adult-onset neurodegenerative disease phenotypes, and thus reducing this effect by 50% may be sufficient to reduce the effect below a threshold necessary to elicit a detectable deficit. Other notable recent studies could also rescue other Tau phenotypes by heterozygous loss of genetic modifiers (Frost et al., 2014; Lasagna-Reeves et al., 2016). While the future identification of inhibitors blocking the Tau-Syngr3 interaction could be useful to titrate the amount of inhibition necessary to rescue functional deficits, the current dataset suggests that partial inhibition of the Tau-Syngr3 interaction may be a feasible and relatively safe therapeutic avenue to pursue.

It is worth noting that wild-type, mutant, and hyperphosphorylated Tau all have identical N-terminal SV-binding domains and, therefore, equal binding affinity to SVs (Zhou et al., 2017); however, it is the pathogenic condition that drives excess Tau to the presynaptic terminal where it binds Syngr3 on SVs, eliciting dominant toxic effects on SV mobility. Given the conservation and specificity of the interaction between Tau and Syngr3, and the observation that some Tau is recovered on SVs from healthy control subjects (Figure 1), it is tempting to speculate that a native interaction between endogenous Tau and Syngr3 may have a physiological function in SV clustering as well. However, our experiments thus far analyzing SV mobility and evoked neurotransmitter release upon the reduction of endogenous Tau (Zhou et al., 2017) or Syngr3 (this study) in wild-type neurons did not reveal a detectable effect, although this does not exclude the possibility of a physiological function of native Tau in SV clustering. It is possible that the loss of Tau or Syngr3 is compensated for by other SV-clustering proteins or that a native role for the Tau-Syngr3 in SV clustering is too subtle to be detected in our experimental paradigms. It is also noteworthy that we observe mostly oligomeric Tau species on SVs from Alzheimer's disease patients, which could potentially be more neurotoxic by simultaneously binding multiple SVs, amplifying the effect of Tau on SV clustering. While a potential physiological function of Tau and Syngr3 should be further investigated, the current dataset is consistent with a primarily gain-of-toxic function mechanism in which Tau mutations or phosphorylation in disease conditions drives the excessive presynaptic localization of Tau, thus allowing it to interact with Syngr3/SVs to elicit presynaptic functional deficits.

Finally, several observations make Syngr3 interesting as a potentially disease-relevant Tau interactor. First, while expressed throughout the brain, Syngr3 expression is enriched in the hippocampus (Belizaire et al., 2004), a region particularly vulnerable to neuronal dysfunction in Alzheimer's disease and Tauopathy mouse models (Braak and Braak, 1991; Yoshiyama et al., 2007). Second, Syngr3 levels are 4-fold higher on glutamatergic SVs compared to GABAergic SVs (Bragina et al., 2010), consistent with a recent report showing that early Tau pathology preferentially affects excitatory neurons (Fu et al., 2017). Third, Syngr3 is also present on extracellular vesicles (Gallart-Palau et al., 2016), which have been proposed as vehicles of cell-to-cell transfer of pathological Tau species spreading throughout the brain (Braak and Braak, 1991; de Calignon et al., 2012; Pickett et al., 2017), a process that is also synapse and activity dependent (Calafate et al., 2015; Thompson et al., 2016; Wu et al., 2016). While these connections are only speculative, they nonetheless poise Syngr3 as an interesting and potentially relevant interactor of Tau warranting further investigation. Importantly, perturbations in synaptic function associated with Tau are thought to drive disease progression, but the contribution of the

presynaptic role of Tau has never been tested experimentally due to lack of a specific approach. Therefore, the identification of Syngr3, an exclusively presynaptic SV protein, provides a new way to assess the contribution of the presynaptic role of Tau to overall neuronal dysfunction, independent of other pathways such as Tau aggregation or Tau localization to postsynapses.

In summary, we uncovered the interaction of Tau with the SV protein Syngr3 as the principle mechanism of Tau binding to presynaptic vesicles, a key step that leads to excessive Tau-induced SV clustering, resulting in restricted SV mobility and ultimately attenuating neurotransmission. Syngr3 is therefore a new culprit in Tau pathogenesis, opening an avenue for the specific targeting of Tau synaptotoxicity in early stages of synaptic and cognitive dysfunction in Alzheimer's disease and related Tauopathies.

STAR★METHODS

Detailed methods are provided in the online version of this paper and include the following:

- KEY RESOURCES TABLE
- CONTACT FOR REAGENT AND RESOURCE SHARING
- EXPERIMENTAL MODEL AND SUBJECT DETAILS
  - Tau PS19 mice
  - Primary mouse hippocampal neurons
  - Fly stocks
  - Human subjects
- METHOD DETAILS
  - Isolation of SVs
  - SDS-PAGE and immunoblotting
  - Purification of recombinant human Tau
  - *In vitro* SV binding assays
  - Liposome flotation assay
  - Tau co-IP and mass spectrometry
  - Immunofluorescence in *Drosophila* larvae
  - FRAP assay of SV mobility
  - Electrophysiology at *Drosophila* larval NMJs
  - Viruses and transduction of primary neurons
  - Immunofluorescence of hippocampal neurons
  - SV dispersion assay
  - Electrophysiology of hippocampal neurons
- QUANTIFICATION AND STATISTICAL ANALYSIS
  - Localization studies at NMJs
  - FRAP analysis of SV mobility at NMJs
  - Localization studies in hippocampal neurons
  - SV dispersion assay
  - Statistics

SUPPLEMENTAL INFORMATION

Supplemental Information includes six figures and two tables and can be found with this article online at https://doi.org/10.1016/j.neuron.2018.01.022.

ACKNOWLEDGMENTS

We thank members of the Verstreken, De Wit, and De Strooper labs for advice. We thank J. Pauwels and F. Impens (VIB Proteomics Core) and K. Vennekens, K. Horré, K. Craessaerts, V. Hendrickx, and J. Verwaeren for assistance. We thank J.T. Littleton for Syngr knockout flies and antibodies. We gratefully acknowledge the patient donors and their families and thank the MRC Edinburgh Brain and Tissue bank. This work was supported by ERC CoG grants to P.V. and T.L.S.-J. (646671) and an ERC StG to J.D.W. (311083), the IWT, the Interuniversity Attraction Pole program by BELSPO (P7/16), a Methusalem grant of the Flemish government (METH/14/07), Opening the Future (LUF), the Fonds voor Wetenschappelijk Onderzoek Vlaanderen (FWO), Odysseus (FWO), IMI (IMPRIND), the UK Dementia Research Institute (Medical Research Council, Alzheimer's Society, and Alzheimer's Research UK), and VIB. P.V. and T.L.S.-J. are members of the FENS Kavli Network of Excellence.

AUTHOR CONTRIBUTIONS

J.M., L.Z., and P.V. conceived the study, designed experiments, analyzed data, and wrote the manuscript. K.W. designed, performed, and analyzed electrophysiology on hippocampal neurons. L.Z. performed electrophysiology at NMJs. J.M. performed all other experiments. A.S., L.B., Y.-C.W., I.-C.S., and N.A. assisted with experiments. K.G. supervised mass spectrometry experiments. T.L.S.-J. provided human tissue samples. I.D., B.D.S., and J.D.W. contributed to study design, analysis of the data, and providing reagents. All authors edited the manuscript and approved the final version.

DECLARATION OF INTERESTS

The authors declare no competing interests.

Received: June 7, 2017
Revised: December 7, 2017
Accepted: January 9, 2018
Published: February 1, 2018

REFERENCES

Ahmed, S., Holt, M., Riedel, D., and Jahn, R. (2013). Small-scale isolation of synaptic vesicles from mammalian brain. Nat. Protoc. *8*, 998–1009.

Allen, M., Kachadoorian, M., Quicksall, Z., Zou, F., Chai, H.S., Younkin, C., Crook, J.E., Pankratz, V.S., Carrasquillo, M.M., Krishnan, S., et al. (2014). Association of MAPT haplotypes with Alzheimer's disease risk and MAPT brain gene expression levels. Alzheimers Res. Ther. *6*, 39.

Ballatore, C., Lee, V.M., and Trojanowski, J.Q. (2007). Tau-mediated neurodegeneration in Alzheimer's disease and related disorders. Nat. Rev. Neurosci. *8*, 663–672.

Bekkers, J.M., and Stevens, C.F. (1991). Excitatory and inhibitory autaptic currents in isolated hippocampal neurons maintained in cell culture. Proc. Natl. Acad. Sci. USA *88*, 7834–7838.

Belizaire, R., Komanduri, C., Wooten, K., Chen, M., Thaller, C., and Janz, R. (2004). Characterization of synaptogyrin 3 as a new synaptic vesicle protein. J. Comp. Neurol. *470*, 266–281.

Bigay, J., Casella, J.-F., Drin, G., Mesmin, B., and Antonny, B. (2005). ArfGAP1 responds to membrane curvature through the folding of a lipid packing sensor motif. EMBO J. *24*, 2244–2253.

Braak, H., and Braak, E. (1991). Neuropathological stageing of Alzheimer-related changes. Acta Neuropathol. *82*, 239–259.

Bragina, L., Giovedì, S., Barbaresi, P., Benfenati, F., and Conti, F. (2010). Heterogeneity of glutamatergic and GABAergic release machinery in cerebral cortex: analysis of synaptogyrin, vesicle-associated membrane protein, and syntaxin. Neuroscience *165*, 934–943.

Brose, N., Hofmann, K., Hata, Y., and Südhof, T.C. (1995). Mammalian homologues of Caenorhabditis elegans unc-13 gene define novel family of C2-domain proteins. J. Biol. Chem. *270*, 25273–25280.

Burgalossi, A., Jung, S., Man, K.-N.M., Nair, R., Jockusch, W.J., Wojcik, S.M., Brose, N., and Rhee, J.-S. (2012). Analysis of neurotransmitter release mechanisms by photolysis of caged Ca^{2+} in an autaptic neuron culture system. Nat. Protoc. *7*, 1351–1365.

Burré, J., Beckhaus, T., Schägger, H., Corvey, C., Hofmann, S., Karas, M., Zimmermann, H., and Volknandt, W. (2006). Analysis of the synaptic vesicle proteome using three gel-based protein separation techniques. Proteomics *6*, 6250–6262.

Caffrey, T.M., and Wade-Martins, R. (2007). Functional MAPT haplotypes: bridging the gap between genotype and neuropathology. Neurobiol. Dis. *27*, 1–10.

Calafate, S., Buist, A., Miskiewicz, K., Vijayan, V., Daneels, G., de Strooper, B., de Wit, J., Verstreken, P., and Moechars, D. (2015). Synaptic Contacts Enhance Cell-to-Cell Tau Pathology Propagation. Cell Rep. *11*, 1176–1183.

Crimins, J.L., Rocher, A.B., and Luebke, J.I. (2012). Electrophysiological changes precede morphological changes to frontal cortical pyramidal neurons in the rTg4510 mouse model of progressive tauopathy. Acta Neuropathol. *124*, 777–795.

de Calignon, A., Polydoro, M., Suárez-Calvet, M., William, C., Adamowicz, D.H., Kopeikina, K.J., Pitstick, R., Sahara, N., Ashe, K.H., Carlson, G.A., et al. (2012). Propagation of tau pathology in a model of early Alzheimer's disease. Neuron *73*, 685–697.

DeKosky, S.T., and Scheff, S.W. (1990). Synapse loss in frontal cortex biopsies in Alzheimer's disease: correlation with cognitive severity. Ann. Neurol. *27*, 457–464.

Depner, H., Lützkendorf, J., Babkir, H.A., Sigrist, S.J., and Holt, M.G. (2014). Differential centrifugation-based biochemical fractionation of the Drosophila adult CNS. Nat. Protoc. *9*, 2796–2808.

DiAntonio, A., Parfitt, K.D., and Schwarz, T.L. (1993). Synaptic transmission persists in synaptotagmin mutants of Drosophila. Cell *73*, 1281–1290.

Frost, B., Hemberg, M., Lewis, J., and Feany, M.B. (2014). Tau promotes neurodegeneration through global chromatin relaxation. Nat. Neurosci. *17*, 357–366.

Fu, H., Rodriguez, G.A., Herman, M., Emrani, S., Nahmani, E., Barrett, G., Figueroa, H.Y., Goldberg, E., Hussaini, S.A., and Duff, K.E. (2017). Tau Pathology Induces Excitatory Neuron Loss, Grid Cell Dysfunction, and Spatial Memory Deficits Reminiscent of Early Alzheimer's Disease. Neuron *93*, 533–541.e5.

Gallart-Palau, X., Serra, A., and Sze, S.K. (2016). Enrichment of extracellular vesicles from tissues of the central nervous system by PROSPR. Mol. Neurodegener. *11*, 41.

Hong, M., Zhukareva, V., Vogelsberg-Ragaglia, V., Wszolek, Z., Reed, L., Miller, B.I., Geschwind, D.H., Bird, T.D., McKeel, D., Goate, A., et al. (1998). Mutation-specific functional impairments in distinct tau isoforms of hereditary FTDP-17. Science *282*, 1914–1917.

Hoover, B.R., Reed, M.N., Su, J., Penrod, R.D., Kotilinek, L.A., Grant, M.K., Pitstick, R., Carlson, G.A., Lanier, L.M., Yuan, L.-L., et al. (2010). Tau mislocalization to dendritic spines mediates synaptic dysfunction independently of neurodegeneration. Neuron *68*, 1067–1081.

Hutton, M., Lendon, C.L., Rizzu, P., Baker, M., Froelich, S., Houlden, H., Pickering-Brown, S., Chakraverty, S., Isaacs, A., Grover, A., et al. (1998). Association of missense and 5′-splice-site mutations in tau with the inherited dementia FTDP-17. Nature *393*, 702–705.

Ittner, L.M., Ke, Y.D., Delerue, F., Bi, M., Gladbach, A., van Eersel, J., Wölfing, H., Chieng, B.C., Christie, M.J., Napier, I.A., et al. (2010). Dendritic function of tau mediates amyloid-beta toxicity in Alzheimer's disease mouse models. Cell *142*, 387–397.

Janz, R., Südhof, T.C., Hammer, R.E., Unni, V., Siegelbaum, S.A., and Bolshakov, V.Y. (1999). Essential roles in synaptic plasticity for synaptogyrin I and synaptophysin I. Neuron *24*, 687–700.

Kasprowicz, J., Kuenen, S., Swerts, J., Miskiewicz, K., and Verstreken, P. (2014). Dynamin photoinactivation blocks Clathrin and α-adaptin recruitment and induces bulk membrane retrieval. J. Cell Biol. *204*, 1141–1156.

Kedra, D., Pan, H.Q., Seroussi, E., Fransson, I., Guilbaud, C., Collins, J.E., Dunham, I., Blennow, E., Roe, B.A., Piehl, F., and Dumanski, J.P. (1998). Characterization of the human synaptogyrin gene family. Hum. Genet. *103*, 131–141.

Koss, D.J., Jones, G., Cranston, A., Gardner, H., Kanaan, N.M., and Platt, B. (2016). Soluble pre-fibrillar tau and β-amyloid species emerge in early human Alzheimer's disease and track disease progression and cognitive decline. Acta Neuropathol. *132*, 875–895.

Labbé, C., Heckman, M.G., Lorenzo-Betancor, O., Soto-Ortolaza, A.I., Walton, R.L., Murray, M.E., Allen, M., Uitti, R.J., Wszolek, Z.K., Smith, G.E., et al. (2016). MAPT haplotype H1G is associated with increased risk of dementia with Lewy bodies. Alzheimers Dement. *12*, 1297–1304.

Lasagna-Reeves, C.A., de Haro, M., Hao, S., Park, J., Rousseaux, M.W.C., Al-Ramahi, I., Jafar-Nejad, P., Vilanova-Velez, L., See, L., De Maio, A., et al. (2016). Reduction of Nuak1 Decreases Tau and Reverses Phenotypes in a Tauopathy Mouse Model. Neuron *92*, 407–418.

Le Guennec, K., Quenez, O., Nicolas, G., Wallon, D., Rousseau, S., Richard, A.-C., Alexander, J., Paschou, P., Charbonnier, C., Bellenguez, C., et al. (2017). 17q21.31 duplication causes prominent tau-related dementia with increased MAPT expression. Mol. Psychiatry *22*, 1119–1125.

Liu, C., Song, X., Nisbet, R., and Götz, J. (2016). Co-immunoprecipitation with Tau isoform-specific antibodies reveals distinct protein interactions and highlights a putative role for 2N Tau in disease. J. Biol. Chem. *291*, 8173–8188.

Piccoli, G., Onofri, F., Cirnaru, M.D., Kaiser, C.J.O., Jagtap, P., Kastenmüller, A., Pischedda, F., Marte, A., von Zweydorf, F., Vogt, A., et al. (2014). Leucine-rich repeat kinase 2 binds to neuronal vesicles through protein interactions mediated by its C-terminal WD40 domain. Mol. Cell. Biol. *34*, 2147–2161.

Pickett, E.K., Henstridge, C.M., Allison, E., Pitstick, R., Pooler, A., Wegmann, S., Carlson, G., Hyman, B.T., and Spires-Jones, T.L. (2017). Spread of tau down neural circuits precedes synapse and neuronal loss in the rTgTauEC mouse model of early Alzheimer's disease. Synapse *71*, e21965.

Polydoro, M., Dzhala, V.I., Pooler, A.M., Nicholls, S.B., McKinney, A.P., Sanchez, L., Pitstick, R., Carlson, G.A., Staley, K.J., Spires-Jones, T.L., and Hyman, B.T. (2014). Soluble pathological tau in the entorhinal cortex leads to presynaptic deficits in an early Alzheimer's disease model. Acta Neuropathol. *127*, 257–270.

Roberson, E.D., Scearce-Levie, K., Palop, J.J., Yan, F., Cheng, I.H., Wu, T., Gerstein, H., Yu, G.-Q., and Mucke, L. (2007). Reducing endogenous tau ameliorates amyloid beta-induced deficits in an Alzheimer's disease mouse model. Science *316*, 750–754.

Rocher, A.B., Crimins, J.L., Amatrudo, J.M., Kinson, M.S., Todd-Brown, M.A., Lewis, J., and Luebke, J.I. (2010). Structural and functional changes in tau mutant mice neurons are not linked to the presence of NFTs. Exp. Neurol. *223*, 385–393.

Sankaranarayanan, S., and Ryan, T.A. (2000). Real-time measurements of vesicle-SNARE recycling in synapses of the central nervous system. Nat. Cell Biol. *2*, 197–204.

Santacruz, K., Lewis, J., Spires, T., Paulson, J., Kotilinek, L., Ingelsson, M., Guimaraes, A., DeTure, M., Ramsden, M., McGowan, E., et al. (2005). Tau suppression in a neurodegenerative mouse model improves memory function. Science *309*, 476–481.

Seabrooke, S., Qiu, X., and Stewart, B.A. (2010). Nonmuscle Myosin II helps regulate synaptic vesicle mobility at the Drosophila neuromuscular junction. BMC Neurosci. *11*, 37.

Spires-Jones, T.L., and Hyman, B.T. (2014). The intersection of amyloid beta and tau at synapses in Alzheimer's disease. Neuron *82*, 756–771.

Stevens, R.J., Akbergenova, Y., Jorquera, R.A., and Littleton, J.T. (2012). Abnormal synaptic vesicle biogenesis in Drosophila synaptogyrin mutants. J. Neurosci. *32*, 18054–18067, 18067a.

Tai, H.-C., Serrano-Pozo, A., Hashimoto, T., Frosch, M.P., Spires-Jones, T.L., and Hyman, B.T. (2012). The synaptic accumulation of hyperphosphorylated tau oligomers in Alzheimer disease is associated with dysfunction of the ubiquitin-proteasome system. Am. J. Pathol. *181*, 1426–1435.

Tai, H.-C., Wang, B.Y., Serrano-Pozo, A., Frosch, M.P., Spires-Jones, T.L., and Hyman, B.T. (2014). Frequent and symmetric deposition of misfolded tau oligomers within presynaptic and postsynaptic terminals in Alzheimer's disease. Acta Neuropathol. Commun. *2*, 146.

Takamori, S., Holt, M., Stenius, K., Lemke, E.A., Grønborg, M., Riedel, D., Urlaub, H., Schenck, S., Brügger, B., Ringler, P., et al. (2006). Molecular anatomy of a trafficking organelle. Cell *127*, 831–846.

Thompson, A.G., Gray, E., Heman-Ackah, S.M., Mäger, I., Talbot, K., Andaloussi, S.E., Wood, M.J., and Turner, M.R. (2016). Extracellular vesicles in neurodegenerative disease - pathogenesis to biomarkers. Nat. Rev. Neurol. *12*, 346–357.

Verstreken, P., Koh, T.-W., Schulze, K.L., Zhai, R.G., Hiesinger, P.R., Zhou, Y., Mehta, S.Q., Cao, Y., Roos, J., and Bellen, H.J. (2003). Synaptojanin is recruited by endophilin to promote synaptic vesicle uncoating. Neuron *40*, 733–748.

Wang, Y., and Mandelkow, E. (2016). Tau in physiology and pathology. Nat. Rev. Neurosci. *17*, 5–21.

Wang, L., Das, U., Scott, D.A., Tang, Y., McLean, P.J., and Roy, S. (2014). α-synuclein multimers cluster synaptic vesicles and attenuate recycling. Curr. Biol. *24*, 2319–2326.

Winder-Rhodes, S.E., Hampshire, A., Rowe, J.B., Peelle, J.E., Robbins, T.W., Owen, A.M., and Barker, R.A. (2015). Association between MAPT haplotype and memory function in patients with Parkinson's disease and healthy aging individuals. Neurobiol. Aging *36*, 1519–1528.

Wu, J.W., Hussaini, S.A., Bastille, I.M., Rodriguez, G.A., Mrejeru, A., Rilett, K., Sanders, D.W., Cook, C., Fu, H., Boonen, R.A.C.M., et al. (2016). Neuronal activity enhances tau propagation and tau pathology in vivo. Nat. Neurosci. *19*, 1085–1092.

Yoshiyama, Y., Higuchi, M., Zhang, B., Huang, S.-M., Iwata, N., Saido, T.C., Maeda, J., Suhara, T., Trojanowski, J.Q., and Lee, V.M.Y. (2007). Synapse loss and microglial activation precede tangles in a P301S tauopathy mouse model. Neuron *53*, 337–351.

Zhao, X., Kotilinek, L.A., Smith, B., Hlynialuk, C., Zahs, K., Ramsden, M., Cleary, J., and Ashe, K.H. (2016). Caspase-2 cleavage of tau reversibly impairs memory. Nat. Med. *22*, 1268–1276.

Zhou, L., McInnes, J., Wierda, K., Holt, M., Herrmann, A.G., Jackson, R.J., Wang, Y.-C., Swerts, J., Beyens, J., Miskiewicz, K., et al. (2017). Tau association with synaptic vesicles causes presynaptic dysfunction. Nat. Commun. *8*, 15295.

STAR★METHODS

KEY RESOURCES TABLE

REAGENT or RESOURCE	SOURCE	IDENTIFIER
Antibodies		
anti-Actin mouse	DSHB	Cat#: JLA20; RRID:AB_528068
anti-ATP synthase mouse	Abcam	Cat#: ab14730; RRID:AB_301438
anti-*Drosophila* Cysteine String Protein (CSP) mouse	DSHB	Cat#: DCSP-2; RRID:AB_528183
anti-*Drosophila* Discs-large (Dlg) mouse	DSHB	Cat#: 4F3; RRID:AB_528203
anti-*Drosophila* Synaptogyrin (Syngr) rabbit	Stevens et al., 2012	RRID:AB_2569703
anti-GAPDH mouse	EMD Millipore	Cat#: MAB374; RRID:AB_2107445
anti-His Tag mouse	Thermo Fisher	Cat#: 37-2900; RRID:AB_2533309
anti-Human Tau "hTau" (HT7) mouse	Thermo Fisher	Cat#: MN1000; RRID:AB_223454
anti-MAP2 chicken	Abcam	Cat#: ab5392; RRID:AB_2138153
anti-Munc18-1 (Munc18) rabbit	Cell Signaling	Cat#: 13414; RRID:AB_10891779
anti-phospho-Tau pSer202/pThr205 (AT8)	Thermo Fisher	Cat#: MN1020; RRID:AB_223647
anti-phospho-Tau pSer396/pSer404 (PHF-1)	Laboratory of Peter Davies	RRID:AB_2315150
anti-PSD-95 rabbit	Cell Signaling	Cat#: 3450T; RRID:AB_2292883
anti-Synapsin-1 (Syn) rabbit	EMD Millipore	Cat#: AB1543P; RRID:AB_90757
anti-Synaptic vesicle glycoprotein 2A (SV2) mouse	DSHB	Cat#: SV2; RRID:AB_2315385
anti-Synaptobrevin-2 / VAMP2 (Syb) mouse	Synaptic Systems	Cat#: 104 211; RRID:AB_887811
anti-Synaptogyrin-3 (Syngr3) mouse	Santa Cruz Biotechnology	Cat#: sc-271046; RRID:AB_10611955
anti-Syngr3 rabbit	Novus Biologicals	Cat#: NBP2-30475
anti-Synaptophysin-1 (Syph) mouse	Synaptic Systems	Cat#: 101 011; RRID:AB_887824
anti-Synaptotagmin-1 (Syt) cytoplasmic epitope mouse	DSHB	Cat#: asv 48; RRID:AB_2199314
anti-Synaptotagmin-1 (Syt) vesicular epitope rabbit	Synaptic Systems	Cat#: 105 102; RRID:AB_887835
anti-Total Tau (DAKO)	DAKO	Cat#: A0024; RRID:AB_10013724
anti-VGlut1 guinea pig	EMD Millipore	Cat#: AB5905; RRID:AB_2301751
Bacterial and Virus Strains		
Lentivirus CMV::RFP, U6::shRNA scramble	This paper	N/A
Lentivirus CMV::RFP, U6::shRNA anti-Syngr3 A	This paper	N/A
Lentivirus CMV::RFP, U6::shRNA anti-Syngr3 B	This paper	N/A
Lentivirus Synapsin::Synaptophysin-eGFP	This paper	N/A
Biological Samples		
Hippocampal tissue samples from human brain	Edinburgh Brain and Tissue Bank	https://www.ed.ac.uk/clinical-brain-sciences/research/edinburgh-brain-and-tissue-bank
Chemicals, Peptides, and Recombinant Proteins		
Recombinant human Tau protein (0N4R isoform)	Zhou et al., 2017	N/A
PreScission protease	GE Healthcare	Cat#: 27084301
Dynabeads protein G for immunoprecipitation	Thermo Fisher	Cat#: 10003D
D-APV	Abcam	Cat#: ab120003
CNQX	Sigma	Cat#: C127
Experimental Models: Organisms/Strains		
Mouse: C57BL/6J	JAX	Cat#: 000664; RRID:IMSR_JAX:000664
Mouse: "Tau PS19" B6;C3-Tg(Prnp-MAPT*P301S)PS19Vle/J	JAX	Cat#: 008169; RRID:IMSR_JAX:008169

(*Continued on next page*)

Continued

REAGENT or RESOURCE	SOURCE	IDENTIFIER
D. melanogaster: UAS-hTau P301L, V337M, or R406W (0N4R isoform, attP2/68A4 insertion site)	Zhou et al., 2017	N/A
D. melanogaster: UAS-Synaptotagmin-GFP	Bloomington Stock Center	Cat#: 6925; RRID:BDSC_6925
D. melanogaster: UAS-syngr shRNA (TRiP.HMS01724)	Bloomington Stock Center	Cat#: 38274; RRID:BDSC_38274
D. melanogaster: *syngr*^{1} knockout	Stevens et al., 2012	Flybase ID# FBal0284662
Oligonucleotides		
shRNA targeting sequence: scramble: GCACTACCAGAGCTA ACTCAGATAGTACT	This paper	N/A
shRNA targeting sequence: mouse Syngr3 A: GTTCGTAGGCT TCTGTTTCCTCACCAATC	This paper	N/A
shRNA targeting sequence: mouse Syngr3 B: GAGCCTGCCG CTTCGGCGTCGTACTAGGT	This paper	N/A
Recombinant DNA		
Plasmid: pGEX_GST-Prescission-Tau-8x-His	Zhou et al., 2017	N/A
Plasmid: pRFP-CB-shLenti	Origene	Cat#: TR30032
Software and Algorithms		
NIS-Elements	Nikon	https://www.nikoninstruments.com
Graphpad Prism 7.0	GraphPad	https://www.graphpad.com
Image Studio Lite	LI-COR Biosciences	https://www.licor.com
ImageJ	NIH	https://imagej.nih.gov/ij/

CONTACT FOR REAGENT AND RESOURCE SHARING

Further information and requests for resources and reagents should be directed to and will be fulfilled by the Lead Contact, Patrik Verstreken (patrik.verstreken@kuleuven.vib.be).

EXPERIMENTAL MODEL AND SUBJECT DETAILS

Tau PS19 mice

All animal studies were performed under the guidelines and approval of the KU Leuven Animal Ethics Committee, which conforms to national and EU FELASA guidelines on animal welfare. Animals were housed in a conventional vivarium with a 12 h light cycle and fed standard chow and water. The generation and characterization of the Tau PS19 mouse model has been previously described (Yoshiyama et al., 2007). PS19 mice expressing human Tau^{P301S} (1N4R isoform) under control of the mouse prion promoter were obtained from JAX (Stock # 008169, strain name: B6;C3-Tg(Prnp-MAPT*P301S)PS19Vle/J). The colony was maintained by mating Tau PS19 hemizygous males to unrelated wild-type C57BL/6 females. Hemizygous Tau PS19 transgenic mice were identified by genotyping using the primers 5′-GGGGACACGTCTCCACGGCATCTCAGCAATGTCTCC–3′ (forward) and 5′–TCCCCCAGCCTAGACCACGA GAAT–3′ (reverse) which gives a hTau^{P301S} transgene-specific PCR product at 350 bp. An internal control primer pair (forward 5′–CAAATGTTGCTTGTCTGGTG–3′, reverse 5′–GTCAGTCGAGTGCACAGTTT–3′), which gives a PCR product at 170 bp, was used as a positive control. DNA from embryonic tails was prepared and processed for genotyping using the KAPA Mouse Genotyping HotStart Kit (KAPA Biosystems) according to manufacturer's instructions.

Primary mouse hippocampal neurons

For primary neuronal cultures, hemizygous Tau PS19 males on a C57BL/6 background were mated with wild-type C57BL/6 female mice from an unrelated colony. Embryos were harvested on day E17.5, and brains isolated and dissected in room-temperature Hank's balanced salt solution (HBSS) + 10 mM HEPES (pH 7.4) to obtain the hippocampi. Hippocampal pieces were incubated with 0.25% trypsin and 0.1 mg/mL DNase in HBSS for 15 min at 37°C, followed by three washes in HBSS before resuspension in prewarmed MEM containing 10% (v/v) horse serum, 33 mM D-glucose, and 1X Pen-Strep (Invitrogen). Hippocampal pieces were gently triturated with glass Pasteur pipettes of decreasing size to obtain a single-cell suspension. Neurons were plated at a density of ~55,000 cells per 18 mm glass coverslip (nitric acid-washed and coated with 0.1 mg/mL poly-lysine and 1 μg/mL laminin). 2-4 h after plating, the medium was replaced with NB-B27 medium (Neurobasal medium + 1x B27 supplement, 0.5 mM Glutamax, 0.2x Pen-Strep, Invitrogen). Neurons were kept in a 37°C incubator with 5% CO_2. 1/3rd of the medium was replaced with fresh medium every 7 days. Neurons from hippocampi of each independent embryo were individually cultured and genotyped (embryonic tails

collected during dissection) to determine Tau PS19 or Non Tg littermate. For establishing primary cultures, embryo gender was not determined as the Tau PS19 strain yields male and female progeny in equal proportions. For functional assays, neurons from Non Tg littermates were used as controls in comparison to neurons hemizygous for the Tau^{P301S} transgene.

Fly stocks

Drosophila melanogaster fly stocks were handled using standard protocols, kept in a 12 h light/dark cycle and fed a standard *Drosophila* diet consisting of cornmeal, agar, yeast, sucrose, and dextrose. All experimental crosses involving the UAS/Gal4 bipartite expression system were kept at 25°C to induce transgene expression. Experiments at the larval neuromuscular junction (NMJ) utilized the motor neuron-specific driver D42-Gal4 and were performed in L3-stage wandering larvae (4-5 days of age). Both male and female larvae were utilized for experiments in equal proportions. We previously described the generation and characterization of wild-type or FTDP-17 clinical mutant 0N4R (383 aa) Tau variants (P301L, V337M, R406W) or N-terminally truncated ΔN_Tau mutants into the 68A4 locus on chromosome III (Zhou et al., 2017). All transgenic flies were kept on the w^{1118} strain background. The D42-Gal4 driver was recombined together with UAS-Tau genes onto chromosome III and, where necessary, additionally combined with the $syngr^{1}$ loss-of-function allele on chromosome II (to give heterozygous $syngr^{+/-}$) or UAS-Synaptotagmin-eGFP on chromosome II. *Syngr* KO flies ($syngr^{1}$ loss-of-function allele, w^{1118} background) were previously generated by and gifted from the J. Troy Littleton lab (Stevens et al., 2012). Control crosses were to wild-type w^{1118} strain for consistency of the genetic background. The UAS-Synaptotagmin-eGFP stock was obtained from the Bloomington Stock Center (stock 6925) and the UAS-*syngr* shRNA stock is HMS01724 from the *Drosophila* Transgenic RNAi project (TRiP, Bloomington stock 38274). Other loss-of-function/knockdown alleles and stocks used in the SV interactor genetic screen include syt^{AD4} (DiAntonio et al., 1993), $synj^{2}$ (Verstreken et al., 2003), UAS-*rph* shRNA (TRiP JF01970, Bloomington stock 25950), $shi^{12\text{-}12B}$ (Kasprowicz et al., 2014), and $pnut^{XP}$ (Bloomington stock 5687).

Human subjects

Post-mortem brain tissue (posterior hippocampal samples) was obtained from the Edinburgh Brain and Tissue Bank at the University of Edinburgh. The use of human tissue samples conformed to national and institutional ethics guidelines and was approved by the Edinburgh MRC Brain and Tissue Bank Ethics Committee and the Academic and Clinical Central Office for Research and Development medical research ethics committee (approval 15-HV-016). Case information for all patient samples used in this study can be found in Table S1.

METHOD DETAILS

Isolation of SVs

Isolation of crude SVs (LP2 fraction) from mammalian brain or *Drosophila* adult fly brain was performed based on protocols (Ahmed et al., 2013) and (Depner et al., 2014), respectively, with modifications. For detailed fractionation centrifugation speeds and times see the respective schematics presented in Figures S1 and S2. All steps of fractionation experiments were carried out on ice or at 4°C. Aliquots of pellets were saved at various steps during fractionation and were lysed in RIPA buffer (150 mM NaCl, 1.0% IGEPAL CA-630/NP-40, 0.5% sodium deoxycholate, 0.1% SDS, 50 mM Tris, pH 8.0, Sigma) containing protease and phosphatase inhibitors and stored at −80°C until analysis. Briefly, frozen (human) or fresh (mouse) brain tissue was chopped into 5 mm^2 cubes, and homogenized in sucrose buffer (320 mM sucrose, 4 mM HEPES pH 7.4, 1X Complete protease inhibitor cocktail (Roche), 1X PhosStop phosphatase inhibitor cocktail (Roche) at a volume of 9 mL per 1 g human brain sample or 3 mL per six-week-old mouse brain (C57BL/6 strain). For fly brains, 5 mL of sieved and collected fly heads were ground in a liquid nitrogen-cooled mortar with a pestle into fine powder and resuspended in 15 mL sucrose buffer per 5 mL adult fly heads. Homogenization was performed using 10 strokes at 600 pm (human and mouse brain) or 900 rpm (fly brain) in a Teflon glass homogenizer. Following pelleting of cell debris and nuclei, synaptosomes were isolated and washed once by resuspension in 10 mL sucrose buffer and re-pelleted. Synaptosomes were hypotonically lysed by resuspension of the synaptosome pellet in 10 volumes of HEPES-buffered water (5 mM HEPES pH 7.4, 1X Protease inhibitor cocktail, 1X Phosphatase inhibitor cocktail and Pepstatin A (Roche, fly samples) and incubated for 30 min at 4°C with rotation. For fly brains, the osmotic shock suspension was homogenized using 3 strokes at 2000 rpm. Following osmotic shock, a 25,000 x g centrifugation step removed mitochondria and large synaptic membrane debris; finally, SVs were collected from the supernatant by centrifugation at 165,000 x g for 2 h. The resulting crude SV pellet (LP2/SV) was resuspended in SV resuspension buffer (5 mM HEPES pH 7.4, 300 mM glycine) and frozen in aliquots at −80°C. Vesicles were quantified according to protein content using the Bradford Quick Start reagent (Bio-Rad). The purity of the LP2/SV fraction was verified by immunoblotting 20 μg of protein from fractionation pellets (lysed in RIPA buffer) or 20 μg vesicle suspension for SV markers or contaminates.

SDS-PAGE and immunoblotting

For denaturation of protein samples, 4X lithium dodecyl sulfate (LDS, Invitrogen) was added to samples to a final concentration of 1X supplemented with 1% β-mercaptoethanol and denatured for 10 min at 70-80°C. Protein samples were separated on NuPAGE 10%, 12% or 4%–12% Bis-Tris mini polyacrylamide gels in MOPS buffer (Invitrogen), or 4%–15% Bis-Tris Criterion TGX midi protein gels in Tris-Glycine-SDS buffer (Bio-Rad). For colloidal Coomassie staining, gels were stained with PageBlue staining solution (Thermo Fisher) according to manufacturer's instructions. For immunoblotting, protein gels were transferred to nitrocellulose

membranes using the TransBlot Turbo transfer system (Bio-Rad). Membranes were blocked in TBS-T (1X Tris-Buffered Saline solution + 0.05% Tween-20) with 5% (w/v) milk powder for 30-60 min at room temperature. Primary antibodies were diluted in blocking buffer (see table below) and incubated with membranes for 1-2 h at room temperature or overnight at 4°C, followed by 4 × 10 min washing in TBS-T. Secondary HRP-conjugated antibodies (Jackson Immunoresearch) were diluted 1:10,000 in blocking buffer and incubated with membranes for 1 h at room temperature, then washed for 6 × 10 min in TBS-T. Immunoblots were developed using the Western Lightning Plus enhanced chemiluminescence kit (Perkin Elmer) and imaged on a Fuji Film imaging system. Densitometry analysis was performed using Image Studio Lite.

Purification of recombinant human Tau

We previously described the purification of soluble recombinant human Tau from bacteria (Zhou et al., 2017). The cDNA sequences encoding human full-length Tau (0N4R isoform, 383 aa) or ΔN_Tau (aa 113-383) were cloned behind a N-terminal GST tag and PreScission Protease cleavage sequence in the pGEX-6P-1 plasmid and was followed by a C-terminal 8x-His tag (inserted into the reverse amplification primer). Sequence-verified plasmids were transformed into Rosetta bacteria (Novagen) and maintained in medium containing ampicillin and chloramphenicol. Overnight pre-cultures were diluted 1:10 into LB medium, incubated for 2 h at 37°C to exponential phase, and then expression was induced by addition of IPTG to a final concentration of 0.4 mM. Expression was carried out for 2 h at 37°C, followed by pelleting of cells (5,000 x g for 15 min); cell pellets were stored at −80°C until use. For purification, all steps were carried out on ice or at 4°C. A cell pellet from a 50 mL bacterial culture was resuspended in 1.5 mL lysis buffer (1X PBS supplemented with 1X protease inhibitor cocktail, Lysozyme, Benzonase, 1% Triton X-100, and 10% glycerol) and incubated for 30 min at 4°C with mixing. Lysates were clarified by centrifugation at 16,000 x g for 20 min, then incubated with 150 μL washed Glutathione Sepharose 4B (GE Healthcare) for 2 h at 4°C. Glutathione Sepharose beads were washed 3 times with PBS supplemented with 250 mM NaCl, and 2 times with PreScission Protease cleavage buffer (20 mM Tris-HCl pH 7.0, 50 mM NaCl, 0.5 mM EDTA, 1 mM DTT, 0.01% Tween-20). Beads were incubated overnight at 4°C with GST-tagged PreScission Protease (GE Healthcare) in cleavage buffer to remove the N-terminal GST tag and liberate Tau from the Sepharose beads. The next morning, the supernatant was incubated for 1 h with 75 μL fresh, washed Glutathione Sepharose to remove any unbound protease or uncleaved Tau. Cleaved Tau-8xHis was then purified against the C-terminal His tag by incubation with 50 uL Ni-NTA resin (Bio-Rad) for 45 min, then washed 3x in His wash buffer (50 mM NaH_2PO_4 pH 8.0, 300 mM NaCl, 20 mM imidazole), and eluted by incubation with His elution buffer for 15 min (same buffer with 250 mM imidazole). Purified Tau was concentrated using an Amicon Centrifugal Filter unit with 10 kDa molecular weight cut-off (Millipore) and quantified using the Bradford Quick Start reagent. Using this method, purification of one 50 mL cell pellet yields approximately 8 μg of soluble Tau with > 95% purity. For all experiments, Tau was always purified freshly and used immediately upon finishing purification.

In vitro SV binding assays

The ability of purified recombinant Tau to bind isolated SVs *in vitro* was assessed using a vesicle sedimentation assay (Piccoli et al., 2014; Zhou et al., 2017). In this assay, 500 ng of freshly purified Tau-8xHis was incubated together with 20 μg (according to protein) isolated SVs in 100 μL SV binding buffer (4 mM HEPES pH 7.4, 5 mM Tris-HCl pH 7.4, 220 mM glycine, 30 mM NaCl, 1X protease inhibitor cocktail) for 2 h at 4°C with rotation. The 100 μL binding reaction was then diluted into 600 μL binding buffer to prevent tubes from breaking during centrifugation. Vesicles were pelleted by ultracentrifugation at 165,000 x g for 1 h, and the pellet was resuspended and denatured in 1X LDS sample buffer. The presence of Tau co-sedimenting together with SVs in the pellet fraction (detected by immunoblotting of the vesicle pellet with anti-His antibody) indicates binding.

Limited proteolysis of SVs was carried out by incubating 75 μg SVs together with 50 μL Sepharose-coupled TPCK-treated trypsin (Thermo Fisher) for 3 h at 37°C. After 3 h, proteolysis was halted by the addition of 1X protease inhibitor cocktail, 1 mM PMSF, and 0.5 mg/mL soybean trypsin inhibitor (Sigma) and the Sepharose-conjugated trypsin was removed by centrifugation at 3,000 x g to remove the Sepharose slurry. As a control, untreated vesicles were incubated at 37°C for 3 h but in the absence of trypsin.

To remove peripheral SV-associated proteins, vesicles were stripped with carbonate (Brose et al., 1995). Isolated SVs were diluted in buffer containing 100 mM Na_2CO_3 pH 11 and 1X protease inhibitors and incubated at 4°C for 30 min. Vesicles were pelleted by ultracentrifugation at 165,000 x g for 1 h then resuspended in neutral buffer (5 mM HEPES pH 7.4, 300 mM glycine). As a control, unstripped vesicles were handled the same except diluted in neutral buffer instead of carbonate buffer. Equal volumes of untreated or carbonate-stripped vesicles were introduced into the binding reaction.

Liposome flotation assay

The liposome flotation assay is based on a protocol previously described (Bigay et al., 2005). To generate small protein-free liposomes 0.25 mg of bovine brain Folch-fraction lipid extract (Avanti Lipids) was dried under a nitrogen stream and desiccated overnight in a vacuum chamber. Liposomes of 30-60 nm diameter were generated by adding 250 μL warmed SV binding buffer to the lipid film and sonicating for 5 min in a 37°C bath. Electron microscopy verified uniform 30-60 nm diameter of liposomes. 64 μg of liposomes was mixed together with 1.5 μg freshly purified Tau in 150 μL SV binding buffer and incubated together for 1 h at 4°C. After 1 h, the density of the binding reaction was adjusted to 30% (w/v) sucrose by addition of 100 μL of a 75% sucrose solution. The 250 μL

binding reaction in 30% sucrose was overlaid with a middle 200 μL layer of 25% sucrose and a top layer of 50 μL SV buffer (no sucrose). The gradient was centrifuged at 240,000 x g for 1 h at 4°C, and then 30 μL fractions from the bottom, middle, or top layers were collected, denatured with LDS and immunoblotted for Tau with anti-His antibodies. Due to their density, liposomes rise to the top sucrose-free fraction during centrifugation, together with any proteins bound to them. Thus, immunoblotting for protein present in the top fraction indicates binding to liposomes.

Tau co-IP and mass spectrometry

SVs isolated from mouse brains (LP2/SV fraction) were lysed in 2% Triton X-100 in SV resuspension buffer (5 mM HEPES pH 7.4, 300 mM glycine) for 1 h at 4°C, followed by clearing of membrane debris and intact vesicles by centrifugation at 165,000 x g for 1 h. The SV lysate was diluted in SV binding buffer to a final concentration of 0.6% Triton X-100 and supplemented with fresh protease inhibitors and NaCl to a final concentration of 100 mM. For co-immunoprecipitation, 2 μg of purified Tau^{FL}-8xHis or $Tau^{\Delta N}$-8xHis was bound to 25 μL of washed Protein G Dynabeads (Invitrogen) using 1 μg mouse anti-His IgG antibody (Thermo Fisher, clone 4A12E4) for 2 h at 4°C. Beads were washed twice then incubated with SV lysate (330 μg protein per reaction, 0.6% Triton X-100, 100 mM NaCl) in SV buffer with 1% BSA and fresh protease inhibitors overnight at 4°C with rotation. As a negative control, we incubated SV lysate together with Dynabeads containing only the anti-His IgG antibody. After the overnight incubation, beads were washed three times with SV buffer + 0.6% Triton X-100 and three times with SV buffer to remove detergents. Samples were immediately processed for mass spectrometry.

Intact Tau-protein complexes were processed using on-bead digestion by overnight incubation with 0.2 mg/mL trypsin in 50 mM ammonium bicarbonate buffer at 37°C. The resulting peptide mixture was dried in a SpeedVac, and the peptide pellet was resuspended in loading solvent (2% acetonitrile, 0.1% trifluoroacetic acid). $1/10^{th}$ of each sample was run in triplicate by LC-MS/MS by 30 min separation on a 2%–50% gradient of solvent (80% acetonitrile, 19.9% water and 0.1% formic acid) coupled to a LTQ-Orbitrap XL mass spectrometer. Peptide spectra were searched with Mascot Daemon software against a *Mus musculus* protein database to identify proteins. The unfiltered mass spectrometry dataset is shown in Table S2. Identified proteins were cross-referenced against comprehensive lists of SV proteins (Burré et al., 2006; Takamori et al., 2006) and were classified as transmembrane SV proteins, peripheral SV proteins, or non-SV proteins (likely contaminates). A filtered list of identified SV-specific proteins absent in the negative control is shown in Figure 3B. Mass spectrometry experiments were performed at the VIB Proteomics Core (University of Ghent, Belgium).

Immunofluorescence in *Drosophila* larvae

For immunofluorescence at *Drosophila* larval NMJs, wandering third-instar (L3) larvae were dissected in freshly prepared HL3 buffer (110 mM NaCl, 5 mM KCl, 10 mM $NaHCO_3$, 5 mM HEPES, 30 mM sucrose, 5 mM trehalose, pH 7.4) on Sylgard-coated plates then fixed in HL3 + 3.7% formaldehyde for 20 min at room temperature. Larvae were gently dissected in calcium-free, low potassium (5 mM KCl) HL3 buffer to avoid stimulation and therefore maintain a tight peripheral distribution of SVs close to the presynaptic membrane. Larval filets were transferred to microcentrifuge tubes, washed with PBS and permeabilized with PBS + 0.4% Triton X-100 for 1 h at room temperature then blocked for 1 h in blocking buffer (PBS + 1% BSA + 0.4% Triton X-100). Primary antibody incubation was performed overnight (1:1000 dilution, see antibody table) in blocking buffer. After overnight incubation, larvae were washed 3 × 20 min (PBS + 0.4% Triton X-100) then incubated for 2 h with Alexa Fluor-488 or −555 antibodies (Invitrogen) diluted 1:1000 in blocking buffer, followed again by washing 3 × 20 min. Larvae were mounted on glass slides using VectaShield Antifade mounting medium (Vector Laboratories). Images of NMJs at segments A2/A3 of larval muscles 12/13 were acquired with a Nikon A1R confocal laser scanning microscope by acquiring Z stacks through the entire NMJ in 0.2 μm depth intervals with a 1.0 Airy unit pinhole opening. All images of NMJs shown are maximum projections of Z stacks.

FRAP assay of SV mobility

The use of a fluorescence recovery after photobleaching (FRAP) assay to assess SV mobility has been described previously (Seabrooke et al., 2010; Zhou et al., 2017). Flies expressing UAS-Synaptotagmin-GFP and UAS-Tau under control of the D42-Gal4 promoter were crossed with wild-type (w^{1118} strain) or *syngr* KO flies to give a *syngr* ± background. Third-instar larvae were dissected in fresh HL3 buffer and pinned down to Sylgard-coated plates. Synaptotagmin-GFP fluorescence was visualized on a Nikon A1R confocal laser microscope with a 60x 1.0 N.A. water immersion objection immersed in HL3 buffer. Images were acquired at 1.12 μs/px, pinhole 1 airy unit, resolution 512 × 512 px using the 488 nm laser line and appropriate filters for GFP fluorescence. All recordings were made from boutons at segments A2/A3 of muscles 12/13. Boutons were selected to ensure flat geometry and similar fluorescence volume and intensity both within the photobleached spot and in the entire bouton. Following acquisition of a pre-bleach baseline, a small spot (24 × 30 px) on the periphery of the bouton was photobleached using 95% laser power of both 405 nm and 488 nm laser lines (9 iterations). Imaging at normal acquisition settings was continued at 1 s intervals for 60 s.

Electrophysiology at *Drosophila* larval NMJs

For electrophysiology, flies expressing D42 > $UAS\text{-}Tau^{P301L}$ (recombined on chromosome III) were crossed to wild-type or *syngr* KO flies to give a $syngr^{+/-}$ background. Larvae were dissected in HL3 buffer on sylgard-coated plates. Stimulation and recordings were performed in room-temperature HL3 buffer supplemented with 0.5-2 mM $CaCl_2$ as indicated in the figure legend. Axons innervating

NMJs at segments A2/A3 of larval muscles at 12/13 were cut and used for intracellular voltage recordings using sharp electrodes (~20 MΩ resistance, 2X stimulation threshold). NMJ miniature or evoked excitatory junction potentials were recorded with an Axoclamp 900A amplifier and digitized with a Digi-data 1440A device, and recorded in pClamp software (version 10.2, Molecular Devices). For 10 Hz stimulation, EJP amplitudes were binned every 30 s and normalized to the amplitude measured in response to the first 15 stimuli.

Viruses and transduction of primary neurons

Scramble and *syngr3* knockdown vectors: Transfer plasmids encoding RFP (CMV promoter) and scramble or anti-mouse/rat *syngr3* shRNAs (U6 promoter) were produced in the pRFP-CB-shLenti plasmid by Origene. The shSyngr3 A targeting sequence is 5′-GTTCGTAGGCTTCTGTTTCCTCACCAATC-3′ and the shSyngr3 B targeting sequence is 5′-GAGCCTGCCGCTTCGGCGTC GTACTAGGT-3′. The shScramble sequence is 5′-GCACTACCAGAGCTAACTCAGATAGTACT-3′. The loop sequence is 5′-TCAA GAG-3′.

Synaptophysin-eGFP vector: The cDNA sequence encoding rat Synaptophysin (307 aa) was cloned upstream of a C-terminal eGFP fusion tag (238 aa) in a second-generation lentiviral transfer plasmid under control of the rat 1.1 kb Synapsin-1 promoter fragment.

Transfer plasmids, the psPAX2 packaging plasmid, and the pMD2.G envelope plasmid (Addgene) were propagated in TOP10 cells (Invitrogen) and plasmid DNA was purified for transfection using a Plasmid Plus Midi Kit (QIAGEN). 1.3×10^7 HEK293T cells (50%–70% confluency) in a T175 flask were transfected with 1 μg pMD2.G, 9 μg psPAX2, and 10 μg transfer plasmid with Lipofectamine-2000 (Invitrogen) according to manufacturer's instructions in DMEM + 2% fetal bovine serum (FBS). 6 h after transfection, the medium was replaced with 15 mL fresh DMEM + 10% FBS. Conditioned medium containing lentiviral particles was collected 48 h after transfection, was passed through a 0.2 μm filter and concentrated using a Amicon Centrifugal Filter Unit with a 100 kDa molecular weight cut-off to a final volume of 1 mL, then was aliquoted, snap-frozen and stored at −80°C until use. The viral titer was empirically tested; in general, 10-20 μL of concentrated lentivirus-containing medium (15 mL from one T175 flask concentrated to 1 mL) was used to transduce ~55,000 neurons on a 18 mm coverslip in a 12-well plate, which routinely gave > 95% transduction efficiency.

Primary hippocampal neurons were transduced on DIV4 or DIV5. Coverslips of neurons were randomly distributed into experimental groups in equal proportions. Half of the culture medium was transferred to a new plate, to which another half of fresh NB-B27 medium was added. 10-20 μL of each lentivirus was added to each coverslip and left for 6 h to infect neurons. After 6 h, the lentivirus-containing medium was completely removed and was replaced with the half-conditioned/half-fresh NB-B27 mix. Medium was not changed again for 7 days following transduction.

Immunofluorescence of hippocampal neurons

DIV 17 neurons were washed once with PBS (with $MgCl_2$ and $CaCl_2$) and fixed (4% paraformaldehyde + 4% sucrose in PBS) for 25 min at room temperature. Neurons were permeabilized and blocked by incubation with 5% goat serum, 2% BSA, 0.3% Triton X-100 in PBS for 1 h at room temperature. Coverslips were incubated with primary antibody (see table for dilutions) overnight at 4°C in PBS with 2% goat serum, 2% BSA and 0.1% Triton X-100. The next day coverslips were washed 3 × 5 min in PBS, then incubated with secondary Pacific Blue, Alexa Fluor-488, −555 or −647 antibodies (Invitrogen) diluted 1:500 in PBS with 2% goat serum, 2% BSA and 0.1% Triton X-100 for 2 h at room temperature. Following 3 × 5 min washes in PBS, coverslips were mounted onto glass slides with VectaShield Antifade mounting medium (Vector Laboratories). Images were acquired on a Nikon A1R confocal microscope with 1 Airy unit pinhole opening. All images of primary neurons shown are single optical sections (0.2 μm depth).

SV dispersion assay

The vesicle dispersion assay to measure SV mobility in primary hippocampal neurons is based on a protocol previously described (Wang et al., 2014). Coverslips of neurons were randomly distributed into experimental groups in equal proportions. Coverslips containing DIV17 hippocampal neurons transduced on DIV4-5 with lentivirus expressing Synaptophysin-eGFP and, where indicated, lentivirus encoding scramble or anti-*syngr3* shRNAs, were transferred out of their medium and bathed for 5 min in recording buffer (25 mM HEPES pH 7.4, 119 mM NaCl, 2.5 mM KCl, 2 mM $CaCl_2$, 2 mM $MgCl_2$, 30 mM glucose) supplemented with 50 μM D-APV (Abcam) and 10 μM CNQX (Sigma) to halt ongoing network activity. Coverslips were transferred into a RC-49MFSH field stimulation chamber (Warner Instruments) and the coverslip was sealed around the edges with oil. Platinum wire electrodes on either side of the recording chamber were connected to the stimulus isolator unit. Room-temperature recording buffer was added to cover the electrodes, and a 60X 1.0 N.A. water-immersion objective was dipped into the chamber. Live imaging was performed on an upright Nikon A1R confocal microscope, using a pinhole opening of 5 Airy units in 1 s intervals using 0.5%–1.0% laser power in the 488 nm laser line with acquisitions in 1 s intervals. Fluorescence was recorded for 30 s to ensure no photobleaching or loss of focus before stimulation began. From 30 s onward, neurons were stimulated for 180 s by delivering 1 ms pulses at 33.3 ms intervals (30 Hz) using a A310 Accupulser (World Precision Instruments) connected to a A365 Stimulus Isolator (World Precision Instruments) set to 50 mA and unipolar mode. All stimulation and acquisition was performed at room-temperature.

Electrophysiology of hippocampal neurons

The establishment of autaptic neuronal cultures has been previously described (Bekkers and Stevens, 1991; Burgalossi et al., 2012). Glass coverslips were coated with agarose, dried and subsequently grid-stamped with a mixture of poly-lysine and rat-tail collagen. Primary astrocytes dissociated from cortices of P0 NMRI mouse pups (Charles River) were cultivated to 60%–70% confluence in a flask (~1 week) containing DMEM + 10% FBS. For island preparation, 25,000 astrocytes were plated per 30 mm glass coverslip in 6-well plates and allowed to form micro-dot islands in DMEM + 10% FBS for 3-5 days. Medium was then exchanged for modified NB-B27 medium (Neurobasal medium + 1x B27 supplement, 0.5 mM Glutamax, 12 mM D-glucose, 25 μm β-mercaptoethanol, 0.2x Pen-Strep, Invitrogen), and 2,500 hippocampal neurons were plated directly onto islands. Where indicated, neurons were transduced with lentivirus on DIV5 for 6 hours, followed by a single one-half volume medium change. Coverslips of neurons were randomly distributed into experimental groups in equal proportions.

Whole-cell voltage clamp recordings were performed on DIV17-19 isolated neurons. The intracellular pipette solution contained 136 mM KCl, 18 mM HEPES, 4 mM Na-ATP, 4.6 mM $MgCl_2$, 4 mM K_2-ATP, 15 mM Creatine Phosphate, 1 mM EGTA and 50 U/mL Phospocreatine Kinase (300 mOsm, pH 7.30). The extracellular solution used during recordings contained 140 mM NaCl, 2.4 mM KCl, 4 mM $CaCl_2$, 4 mM $MgCl_2$, 10 mM HEPES, 10 mM glucose (300 mOsm, pH 7.30). Neurons were whole-cell voltage clamped at 70 mV using a double EPC-10 amplifier (HEKA Elektronik, Lambrecht/Pfalz, Germany) under control of Patchmaster v2 × 32 software (HEKA Elektronik). Currents were recorded at 20 Hz and low-pass filtered at 3 kHz when stored. Pipettes were pulled using a Sutter P-1000 and resistance ranged from 3 to 5 MΩ. The series resistance was compensated to 75%–85%. Cells with series resistances above 15 MΩ were excluded for analysis. Spontaneous glutamatergic release was (sEPSC) was recorded at −70 mV. Evoked release was induced using brief depolarization of the cell soma (from 70 to 0 mV for 1 ms) to initiate action potential-dependent glutamatergic release (eEPSCs). All recordings were performed at room temperature.

QUANTIFICATION AND STATISTICAL ANALYSIS

Localization studies at NMJs

To quantify the association between Tau and CSP-labeled SVs *in vivo* at *Drosophila* NMJs, we used the "Colocalisation Test" plug-in in ImageJ software. Each bouton at an NMJ was individually encircled as an ROI, and the Z-position was selected where CSP was the widest/most peripheral around the bouton. The "Colocalisation Test" plug-in (ImageJ) was run to measure the overlap between the Tau (DAKO antibody) and CSP channels using 75 iterations and measuring only on the individual Z section. The R(obs) value was taken as the Pearson's colocalization coefficient. To account for the high baseline Pearson coefficient value due to the large area of the bouton occupied by CSP-labeled SVs, we also calculated the Pearson coefficient between CSP and a Fay-randomized (random noise) image generated by the colocalization test plug-in to simulate the baseline colocalization value between CSP and a completely diffuse signal. This value was subtracted from the measured CSP-Tau Pearson coefficient to calculate the relative co-localization value (control set to 1). The same analysis was performed for every bouton at a given NMJ and averaged to give n = 1 data point per NMJ.

FRAP analysis of SV mobility at NMJs

The intensity of the bleached spot, plotted as percent of initial fluorescence, was normalized to a non-bleached reference bouton and measured using Nikon analysis software (NIS-Elements AR 4.5), and the trace was fit to a double-exponential curve in GraphPad Prism 7 software. FRAP traces from 2-4 boutons were acquired per larvae.

Localization studies in hippocampal neurons

The quantification of the presynaptic localization of Tau in hippocampal neurons was measured as the Pearson colocalization coefficient between $hTau^{P301S}$ (HT7 antibody) and the SV marker Synapsin. Entire axon segments of approximately 20 μm were selected as ROIs. Distal axon segments (at least 60 μm away from cell body) were randomly chosen using Synapsin and RFP channels in an unbiased way. The "Colocalisation Test" plug-in in ImageJ was then run on acquired images to measure the overlap between the two channels using 75 iterations and Fay randomization. The R(obs) value was taken as the Pearson's coefficient.

Quantification of $hTau^{P301S}$ levels (HT7 antibody) in axons (using same images as for presynaptic localization) was performed in ImageJ by measuring the fluorescence integrated density along axon segments (approximately 20 μm) selected as ROIs. Quantification of Syaptogyrin-3 levels were performed by measuring Syngr3 integrated density at Synapsin-labeled presynaptic puncta. The relative intensity of 5-10 puncta per axon/cell was normalized to the Synapsin signal and then averaged to give n = 1 data point per cell. Quantification of synapse size was performed by quantifying the area of Synapsin puncta in ImageJ. Quantification of synapse number was manually counted as a function of axon segment length.

SV dispersion assay

For each recording, the change in Synaptophysin-GFP puncta fluorescence intensity (t_0 was set to 100%) was quantified from 20-40 synapses (all distinct Syph-eGFP puncta in view for each coverslip were selected as individual ROIs using Nikon software) from 2-5 axons in view and averaged to give n = 1 averaged trace per coverslip.

Statistics

All statistical analyses were performed with GraphPad Prism 7.0 software. Where quantifications are shown, the graph representation and error bars are defined in each legend, together with the definition of n and which statistical test was performed. Error bars either depict standard deviation (SD) or standard error of the mean (SEM), as indicated in the figure legend. In all instances, statistical significance was defined as follows: n.s. - not significant ($p > 0.05$), * $p < 0.05$, ** $p < 0.01$, *** $p < 0.001$. For multiple comparisons using one-way ANOVA, Dunnett's multiple comparisons test was used to compare each condition to a single control group. For two-way ANOVA, Sidak's multiple comparisons test was used to test genotype as source of variance. No outlier analysis was performed or data points excluded. Sample size was chosen according to that used for similar experiments in previously published literature. Experimenters were not blinded to experimental condition during data acquisition or quantification.